

People's Democratic Republic of Algeria
Ministry of Higher Education and Scientific Research
University M'Hamed BOUGARA – Boumerdes



Institute of Electrical and Electronic Engineering
Department of Electronics

Final Year Project Report Presented in Partial Fulfilment of the
Requirements for the Degree of

‘MASTER’

In Telecommunication
Option: Telecommunications

Title:

**Analysis and Design of MIMO Microstrip
Antennas for Smart Grid Applications**

Presented By:

- **LAMRI Isam Eddine**
- **ZERAIB Ahmed**

Supervisor:

M. DEHMAS

Co-supervisor:

Dr A. MANSOUL

Registration Number:...../2019

Acknowledgments

All praise is due to Allah, and Allah's Peace and Blessings be upon His Final Messenger, his pure family, his noble Companions, and all those who follow them with righteousness until the Day of Judgment.

It is our pleasure to thank those who made this thesis possible.

First and foremost, I offer my sincerest gratitude to **Mr. DEHMAS Mokran** and **Mr. MANSOUL Ali**. Their continuous support, guidance, motivation and time spent explaining things clearly and simply were fundamental for the realization of this work.

We extend our sincere thanks to **Pr. AZRAR Arab**, **Pr. DAHIMEN** and **Pr. M. CHALLAL** for their constant guidance and encouragement during our cursus as a telecommunication student.

We wish to dedicate this thesis to all my colleagues and friends that encouraged, motivated, challenged me and created a very good environment that made these university years memorable.

Last but not least, we are extremely grateful to all my family, specially my parents and brothers, for the help, support and love shared through these five years of university.

Isam Eddine and Ahmed

Abstract

Wireless communications have been growing extensively during the last few decades. This has made possible implementation of Smart Grid systems with a capacity to transmit information from and to power consumers to achieve very high efficiency as well as high data transmission speed.

In this work, an UWB and a Dual Band 2x2 element MIMO microstrip antennas are proposed for these applications. These antennas, printed on an FR-4 dielectric material, are fed by a microstrip line for the UWB and by a coplanar waveguide for the Dual Band structures.

The structures radio electric properties including S-parameters, current distributions, radiation patterns, correlation coefficients and diversity gains were investigated using the CST electromagnetic simulator.

Prototypes of the two final four-element MIMO structures have been fabricated and their S-parameters measured where an agreement is observed between simulated and measured results

Table of content

| | |
|---|------------|
| Acknowledgments | i |
| Abstract | ii |
| List of figures | v |
| List of Abbreviations | vii |
| General Introduction | 1 |
| Chapter 1: Overview on Smart Grids, Microstrip Patch Antennas and MIMO System. | |
| 1.1 Introduction | 2 |
| 1.2 Smart Grids | 2 |
| 1.2.1 WiMAX for Smart Grid applications | 4 |
| 1.2.2 Wi-Fi for Smart Grid applications | 5 |
| 1.3 Microstrip Patch Antennas | 5 |
| 1.3.1 Microstrip Patch Antennas Geometry | 6 |
| 1.3.2 Basic Principles of Operation..... | 6 |
| 1.3.3 Feeding techniques | 7 |
| 1.3.4 Fundamental antenna parameters | 10 |
| 1.3.5 Methods of Analysis..... | 13 |
| 1.4 MIMO systems | 14 |
| 1.4.1 MIMO antennas special parameters: | 16 |
| 1.5 Conclusion | 16 |
| Chapter 2: Ultra Wide Band MIMO Antenna. | |
| 2.1 Introduction | 17 |
| 2.2 Geometry and simulation of reference element | 17 |
| 2.2.1 Basic antenna Structure | 17 |
| 2.2.2 Antenna improvement and optimization | 18 |
| 2.3 Design and simulation of two-element MIMO antenna | 24 |
| 2.4 Design and simulation of a four-element MIMO antenna | 29 |
| 2.5 MIMO antenna system prototypes measurements | 36 |
| 2. 6 Conclusion | 40 |
| Chapter 3: Dual Band MIMO antenna. | |
| 3.1 Introduction | 41 |

| | |
|--|-----------|
| 3.2 Design and simulations of the reference element | 41 |
| 3.3 Design and simulation of four-element MIMO antenna..... | 47 |
| 3.4 MIMO antenna system prototypes measurements. | 53 |
| 3.4 Conclusion..... | 55 |
| General Conclusion..... | 56 |
| References..... | 57 |

List of figures

Chapter 1: Overview on Smart Grids, Microstrip Patch Antennas and MIMO System.

| | |
|--|----|
| Figure 1. 1 A model set up of smart grid network. | 3 |
| Figure 1. 2 An Example of the Smart Metering Structure. | 3 |
| Figure 1. 3 Patches common shapes..... | 6 |
| Figure 1. 4 Cross section of a patch antenna in its basic form. | 6 |
| Figure 1. 5 Microstrip line feed..... | 8 |
| Figure 1. 6 Coaxial Probe Feed | 8 |
| Figure 1. 7 Proximity coupled Feed. | 9 |
| Figure 1. 8 Aperture coupled feed | 9 |
| Figure 1. 9 Coplanar Waveguide (CPW) feed | 9 |
| Figure 1. 10 Three and two-dimensional power patterns | 13 |
| Figure 1. 11 MIMO 2x2 system, graphical representation | 14 |
| Figure 1. 12 Building Blocks of a MIMO system..... | 15 |

Chapter 2: Ultra Wide Band MIMO Antenna.

| | |
|--|----|
| Figure 2. 1 Circular microstrip UWB antenna | 17 |
| Figure 2. 2 Reflection coefficient of the basic UWB antenna | 18 |
| Figure 2. 3 Slotted Ground plane of the antenna..... | 18 |
| Figure 2. 4 Reflection coefficient of the antenna with a slotted ground | 19 |
| Figure 2. 5 Antenna structure after adding square slots | 19 |
| Figure 2. 6 Reflection coefficient of the slotted patch antenna..... | 20 |
| Figure 2. 7 Final antenna structure..... | 20 |
| Figure 2. 8 Reflection coefficient of the reference UWB antenna..... | 21 |
| Figure 2. 9 Simulated gain vs. frequency of the reference UWB antenna..... | 21 |
| Figure 2. 10 Surface current distribution of the reference UWB antenna..... | 22 |
| Figure 2. 11 3-D Radiation pattern of the reference UWB antenna..... | 23 |
| Figure 2. 12 2-D Radiation pattern for 3.5 and 5.8 GHz of the reference UWB antenna..... | 23 |
| Figure 2. 13: Two parallel UWB antenna configuration..... | 24 |
| Figure 2. 14 S-parameters of two parallel UWB antennas..... | 25 |
| Figure 2. 15 Correlation coefficient of two parallel UWB antennas | 25 |
| Figure 2. 16 Diversity gain of two parallel UWB antennas | 26 |
| Figure 2. 17 S-parameters of two parallel UWB antennas with a spacing of 10 mm | 26 |
| Figure 2. 18 Correlation coefficient of two parallel UWB antennas with a spacing of 10 mm..... | 27 |
| Figure 2. 19 Diversity gain of two parallel UWB antennas with a spacing of 10 mm | 27 |
| Figure 2. 20 Two orthogonal UWB antenna configuration | 28 |
| Figure 2. 21 S-parameters of two orthogonal UWB antennas | 28 |
| Figure 2. 22 Correlation coefficient of two orthogonal UWB antennas | 29 |
| Figure 2. 23 Diversity gain for two orthogonal UWB antennas | 29 |
| Figure 2. 24 Configuration of the 4-element UWB MIMO antenna..... | 30 |
| Figure 2. 25 S-parameters of UWB MIMO antenna at “port 1” | 31 |
| Figure 2. 26 Simulated gain vs. frequency of the 4-element UWB MIMO antenna | 31 |

| | |
|--|----|
| Figure 2. 27 Correlation coefficient between adjacent ports | 32 |
| Figure 2. 28 Correlation coefficient between oblique ports | 32 |
| Figure 2. 29 Diversity Gain between adjacent ports | 33 |
| Figure 2. 30 Diversity gain between oblique ports | 33 |
| Figure 2. 31 Surface current distribution of the 4-element UWB antenna | 34 |
| Figure 2. 32 3-D radiation pattern of the UWB MIMO antenna..... | 35 |
| Figure 2. 33 2D radiation pattern at different frequencies when exciting “port 1”..... | 35 |
| Figure 2. 34 Manufactured UWB 2×2 UWB MIMO antenna | 36 |
| Figure 2. 35 prototype after soldering the connectors..... | 37 |
| Figure 2. 36 Setup for two ports reflection coefficients measurement | 37 |
| Figure 2. 37 Measured and simulated $ S_{ij} _{i \neq j}$ coefficients | 39 |
| Figure 2. 38 Measured and simulated reflection coefficients | 39 |

Chapter 3: Dual Band MIMO antenna.

| | |
|---|----|
| Figure 3. 2 Basic Dual Band antenna element geometry | 41 |
| Figure 3. 3 Simulated reflection coefficient of the microstrip antenna for different feed gaps h With $G_L=12$ mm and $S_L=28$ mm..... | 42 |
| Figure 3. 4 Simulated reflection coefficient of the microstrip antenna for different G_L with $h=3.75$ mm $S_L=28$ mm | 42 |
| Figure 3. 5 Simulated reflection coefficient of the microstrip antenna for different S_L with $h=3.75$ mm and $G_L=14.3$ mm..... | 43 |
| Figure 3. 6 Final Dual Band antenna element geometry | 43 |
| Figure 3. 7 Reflection coefficient of the basic Dual Band antenna..... | 44 |
| Figure 3. 8 Simulated gain vs. frequency of the reference Dual Band antenna | 44 |
| Figure 3. 9 Surface current distribution of the reference Dual Band antenna..... | 45 |
| Figure 3. 10 3-D Radiation pattern of the reference Dual Band antenna..... | 46 |
| Figure 3. 11 2-D Radiation pattern of the reference Dual Band antenna at frequencies 3.5 and 5.6 GHz | 46 |
| Figure 3. 12 Configuration of the 4-element Dual Band MIMO antenna..... | 47 |
| Figure 3. 13 S-parameters of the 4-element Dual Band MIMO Antenna | 48 |
| Figure 3. 14 Simulated gain vs. frequency of the 4-element Dual Band MIMO antenna..... | 48 |
| Figure 3. 15 Correlation coefficient between adjacent ports | 49 |
| Figure 3. 16 Correlation coefficient between oblique ports | 49 |
| Figure 3. 17 Diversity gain between adjacent ports | 50 |
| Figure 3. 18 Diversity gain between oblique ports | 50 |
| Figure 3. 19 Surface distribution current of 4-element Dual Band MIMO antenna | 51 |
| Figure 3. 20 3-D radiation pattern of the Dual Band MIMO antenna..... | 52 |
| Figure 3. 21 2-D radiation pattern at different frequencies when exciting “port 1” | 52 |
| Figure 3. 22 Manufactured Dual Band 2×2 MIMO antenna..... | 53 |
| Figure 3. 23 Antenna prototype after soldering the connectors. | 53 |
| Figure 3. 24 Measured and simulated $ S_{ij} _{i \neq j}$ parameters..... | 54 |
| Figure 3. 25 Measured and simulated reflection coefficients | 55 |

List of Abbreviations

ABW: Absolute Bandwidth

BW: Bandwidth

CDTA: Centre du Développement des Technologie Avancée

CPW: Coplanar Waveguide

DSL: Digital Subscriber Line.

FBW: Fractional Bandwidth

FCC: Federal Communications Commission

FDTD: Finite Differences in the Time Domain

FR4: Flame Resistant 4

MAN: Metropolitan Area Networks

MIMO: Multiple-Input Multiple-Output

MISO: Multiple-Input Single-Output

OFDM: Orthogonal Frequency Division Multiple Access.

PC: Personal Computer

SG: Smart Grids

SIMO: Single-Input Multiple-Output

SISO: Single-Input Single-Output

SMA: Sub Miniature version A

SNR: Signal to Noise Ratio

UWB: Ultra-Wideband

VSWR: Stands for Voltage Standing Wave Ratio

Wi-Fi: Wireless Fidelity

WiMAX: Worldwide Interoperability for Microwave Access

WSN: Wireless Sensor Network

ISM: Industrial Scientific and Medical devices

General Introduction

Smart grid technology is expected to play an important role in future challenges related to efficient power consumption and cleaner air. A smart grid is a self-correct system with the ability to provide real time electricity cost. These systems use wireless communication technology for high speed data transmission and cost effective [1].

A typical wireless system consists of different parts among which antenna represents a fundamental unit. Smart Grid can use many wireless communication technologies and frequency bands among which WiMAX (Worldwide Interoperability for Microwave Access) [2] and Wi-Fi (Wireless Fidelity) [3].

The present work aims and deals with design and simulation of an ultra-wide band (UWB) and a Dual Band four element MIMO microstrip antennas dedicated to smart grid systems and operating in WiMAX and Wi-Fi frequency bands. These antennas are printed on an FR-4 dielectric material and they are fed by a microstrip line for the UWB and, by a coplanar waveguide for the Dual Band structures.

The simulations which concern various single element and MIMO antenna characteristics are carried out using the CST Microwave Studio software. The final structures are also fabricated and tested.

The first chapter of this document presents an overview on smart grid systems, microstrip antennas and characteristics, and MIMO (Multiple Input Multiple Output) systems.

The second and third chapters deal with the UWB and the Dual Band structures respectively. They describe in details the steps involved in the design and the analysis processes leading to the final 2x2 element MIMO configurations.

Finally, a conclusion is provided at the end of the report.

Overview on Smart Grids, Microstrip Patch Antennas and MIMO Systems

1.1 Introduction

A smart grid (SG), which includes wireless technology and smart meters, is needed for power efficiency and safety. Smart grids are based on real-time communication to optimize energy delivery and storage and prevent losses. To this end, wireless remote monitoring and control units are used. For communication between different parts involved in smart grid, antennas will be needed. Microstrip antennas are widely used in wireless systems and smart grids. Also, for reduced multipath limitation and enhanced capacity, Multiple-Input Multiple-Output (MIMO) systems are more suitable [4].

1.2 Smart Grids

A Smart Grid is an electrical network that can intelligently integrate the effects of all users including generators and consumers in order to efficiently and safely deliver sustainable and economic energy [5]. A Smart Grid employs innovative products and services together with intelligent monitoring, control, communication, and self-healing technologies to [6-7]:

- Better facilitate the connection and operation of generators of all sizes and technologies.
- Allow consumers to play a part in optimizing the operation of the system.
- Provide consumers with greater information and choice of supply.
- Significantly reduce the environmental impact of the whole electricity supply system.
- Deliver enhanced levels of reliability and security of supply.

A Smart Grid model including smart generation, transmission, storage, smart sensors is shown in figure 1.1.

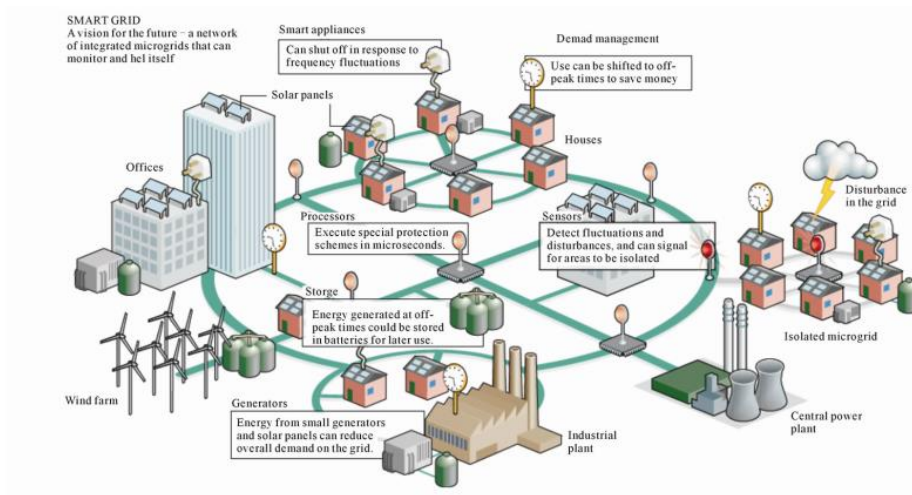


Figure 1. 1 A model set up of smart grid network [7]

Wireless communication plays an important role in realizing the objectives of Smart Grids. Advancements in wireless communication technologies have made it possible to implement a Smart Grid with its capability to conduct various information from and to energy consumers, to achieve a very high utility efficiency. A wireless sensor network (WSN) forms an essential part in realizing a Smart Grid, since it has the ability to construct a highly reliable and self-healing power grid that can quickly react to the events with appropriate actions [8]. A Wireless communication network is needed for information flow in a smart grid system. A smart meter is an electrical meter that records consumption in constant time intervals, one hour or less, and sends the information for monitoring and billing purposes. Also, a smart meter can disconnect-reconnect remotely and control the user appliances and devices to manage loads and demands within the future smart-buildings [9].

Figure 1.2 shows a typical usage scenario for smart meters.

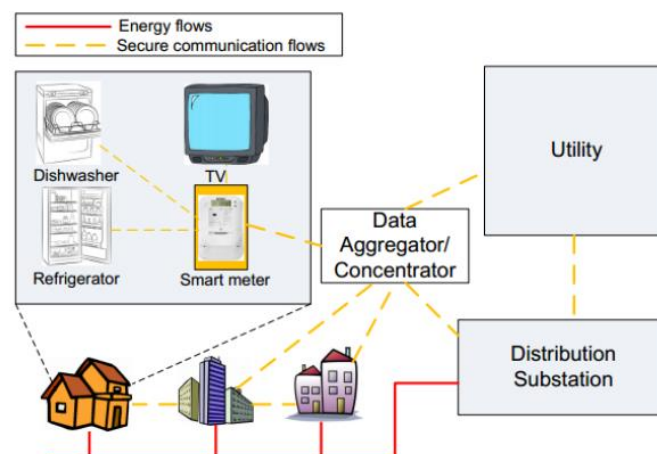


Figure 1. 2 Example of a Smart Metering Structure [10]

The smart meter collects the power consumption information of the dishwasher, TV, and the refrigerator, and also sends the control commands to them if necessary. The data generated by the smart meters in different buildings is transmitted to a data aggregator. This aggregator could be an access point or gateway. This data can be further routed to the electric utility or the distribution substation.

Nevertheless, there are key limiting factors that should be taken into account in the smart metering deployment process, such as time of deployment, operational costs, the availability of the technology and rural/urban or indoor/outdoor environment, etc. In the following, some of the smart grid communications technologies along with their advantages and disadvantages are briefly explained.

1.2.1 WiMAX for Smart Grid applications

Worldwide Interoperability for Microwave Access (WiMAX) is the first commercially available 4G technology. It is ideally suited to meeting both the requirements of smart grid application and the needs of utilities to keep complexity under control without sacrificing security or reliability.

WiMAX is based on the standard IEEE 802.16. and was built especially for communications in Metropolitan Area Networks (MAN) as it offers very high transmission rates at a larger range than other wireless protocols. It was developed at a time when there was substantial interest in a technology that could provide an alternative for the wired communication through DSL (Digital Subscriber Line) for broadband access. The advantages delivered by the IEEE 802.16 over other communication technologies are the following: it overcomes the physical limitation of wired technologies, reasonable cost, broadband access services for a wide selection of devices, high speed and wide range of coverage. The WiMAX Physical Layer offers broadcast access for both mobile and fixed applications [12].

The IEEE 802.16 WiMAX standard allows data transmission using multiple wireless broadband frequency ranges. The original 802.16a standard specified transmissions in the range 10 - 66 GHz, but 802.16d allowed lower frequencies in the range 2 to 11 GHz. The lower frequencies used in the later specifications means that the signals suffer less from attenuation and therefore they provide improved range and better coverage within buildings. This brings many benefits to those using these data links within buildings and means that external antennas are not required.

Different bands are available for WiMAX applications in different parts of the world. The frequencies commonly used are 3.5 and 5.8 GHz for 802.16d and 2.3, 2.5 and 3.5 GHz for 802.16e [13].

1.2.2 Wi-Fi for Smart Grid applications

Wi-Fi technology will certainly be part of any future Smart Grid. Wi-Fi is cost effective, scalable to cover large geographies and many endpoints, and requires no new cabling within the home. Wi-Fi is the dominant home wireless networking standard and thus plays a central role in the Home Area Network for Smart Grid. Wi-Fi is already integrated into home routers, set top boxes, high definition televisions, notebook PCs and smart phones. Wi-Fi enabled thermostats, refrigerators, and washing machines make perfect sense. Whether as a separate network or integrated into existing home networks, Wi-Fi should be the primary Home Area Network for the Smart Grid.

Wi-Fi operates in unlicensed spectrum and so is subject to interference. However, Wi-Fi is designed to operate in this uncontrolled spectrum and is resilient to many types of interference. Wi-Fi coexists very well with other technologies that share these bands.

Originally the 2.4GHz band was favored for Wi-Fi, but as the technology for the 5GHz band (frequency ranges 5.15–5.35 GHz, 5.47–5.725 GHz, and 5.725–5.875 GHz) [13] fell it came into much greater use in view of its wider channel bandwidth capability. It will be seen that many of the 5 GHz Wi-Fi channels fall outside the accepted ISM (Industrial Scientific and Medical devices) unlicensed band and as a result various restrictions are placed on operation at these frequencies.

1.3 Microstrip Patch Antennas

The microstrip patch and other printed antennas are now commonplace as they are readily combined with electronic components and integrated circuits. The feed line can be incorporated into existing microstrip line circuitry branching to amplifiers, mixers, downconverters and semiconductor sources. Another major advantage of the microstrip patch is that it can be flush-mounted planar or conformal with other surfaces, such as an aero foil, with only a minimum of space required for the feed line. The patch may be fed by a transmission line also etched on the dielectric sheet (substrate) or by a probe through the back of the ground plane. The shape of the patch varies significantly although the basic radiation mechanism is similar. One or more resonances can be established in part of the geometry that is coupled to the input. From these resonances, radiation can be

created with different radiation characteristics depending on the geometry, and this has resulted in a variety of useful designs [14].

1.3.1 Microstrip Patch Antennas Geometry

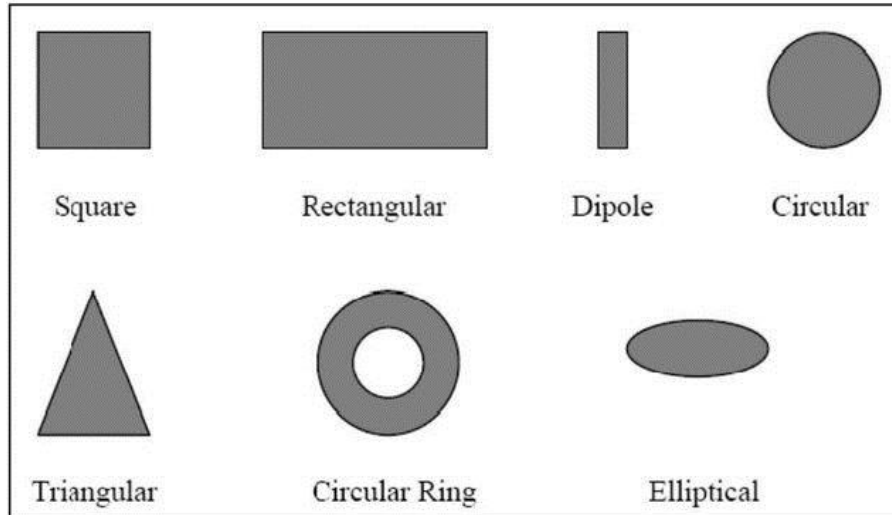


Figure 1. 3 Patches common shapes [15]

In order to simplify analysis and performance prediction, the patch is generally square, rectangular, circular, triangular, and elliptical or some other common shape as shown in figure 1.3. For a rectangular patch, the length L of the patch is usually $0.33 \lambda_0 < L < 0.5 \lambda_0$, where λ_0 is the free space wavelength. The patch is selected to be very thin such that $t \ll \lambda_0$ (where t is the patch thickness). The height h of the dielectric substrate is usually $0.003 \lambda_0 \leq h \leq 0.05 \lambda_0$. The dielectric constant of the substrate (ϵ_r) is typically in the range $2.2 \leq \epsilon_r \leq 12$ [16].

1.3.2 Basic Principles of Operation

Figure 1.4 shows a patch antenna in its basic form: a flat plate over a ground plane. This antenna is often built of printed circuit board material and the substrate makes up the patch antennas dielectric [17].

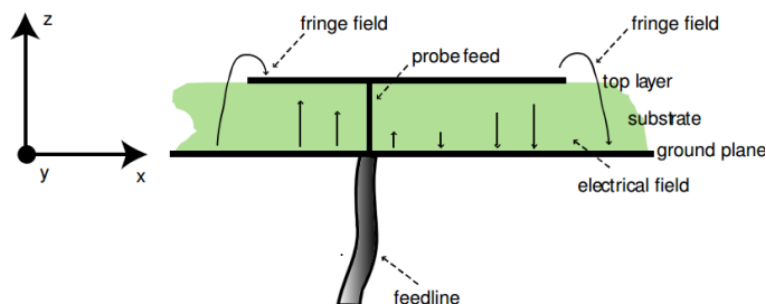


Figure 1. 4 Cross section of a patch antenna in its basic form [17]

The distance between the patch and the ground plane, the substrate or dielectric height h , determines the bandwidth. A thicker substrate increases the gain to some extent, but may lead to undesired effects like surface wave excitation: surface waves decrease efficiency and perturb the radiation pattern. The ground plane should extend beyond the edges of the patch by at least 2 to 3 times the board thickness for proper operation. A ground plane that is too small will result in a reduced front to back ratio. Making the ground plane larger also increases the gain, but as the ground plane size increases, diffraction near the edges plays less of a role and increasing the size of an already large ground plane has very little effect on gain.

In the antenna in figure 1.4, the center conductor of a coaxial line serves as the feed probe to couple electromagnetic energy in and/or out of the patch. A thicker substrate leads to a longer feed probe, a larger feed probe inductance and a degradation of impedance matching. This can be compensated by using a different feed type.

A half wave long patch operates in what we call the fundamental mode: the electric field is zero at the center of the patch, maximum (positive) on one side, and minimum (negative) on the opposite side. These minima and maxima continuously change side like the phase of the RF signal.

The electric field does not stop abruptly near the patch's edges like it would in a cavity: the field extends beyond the outer periphery. These field extensions are known as fringing fields and cause the patch to radiate [18].

1.3.3 Feeding techniques

Patch antennas may be powered using different methods. These are classified in two categories:

- **Contact feeding:** the feeding technique is powered by means of a connecting element such as a microstrip line into the radiating patch.
- **Non-contact feeding:** a transfer of power between the microstrip line and radiating element is performed with the electromagnetic field coupling.

The most famous feeding techniques employed in the microstrip patch antenna are: coaxial probe, feeding technique with microstrip line and aperture or proximity coupling methods [19].

▪ Microstrip Line Feed

In this kind of feeding process in figure 1.5, the edge of the microstrip patch is connected directly to a conducting strip. This feeding method offers the benefit that the conducting line can have the opportunity of engraved on same substrate of patch antenna providing a planar shape [20].

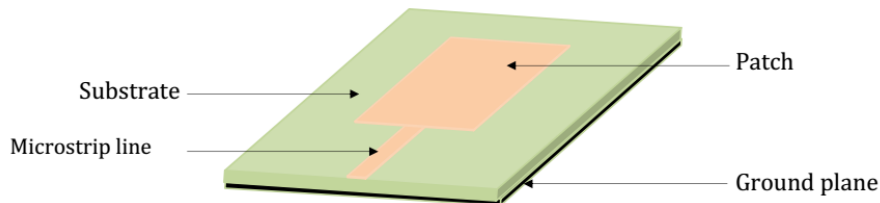


Figure 1. 5 Microstrip line feed [21]

▪ Coaxial Probe Feed

The outside conductor of a coaxial connector attached at ground plane, while the inside is extended across the dielectric and is welded at the radiating element antenna. However, the disadvantage of this technique is a difficult to model and produce narrow bandwidth. Figure 1.6 shows this type of feed technique [20].

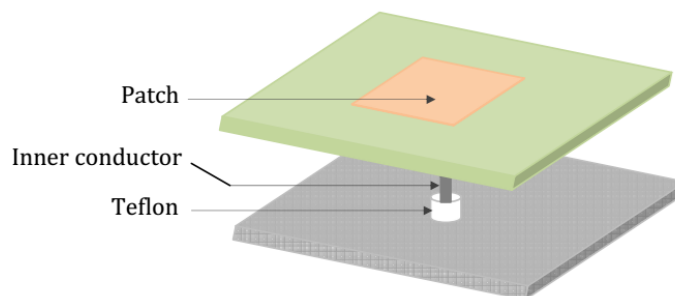


Figure 1. 6 Coaxial Probe Feed [21]

▪ Proximity coupled feed

This feeding technique utilized two dielectric substrates in order that the feed line, firstly, is between two substrates and on the other hand the radiating element is on top of the upper substrate [20] as shown in figure 1.7.

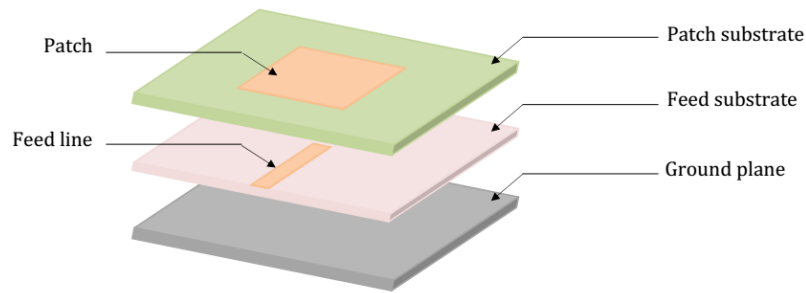


Figure 1. 7 Proximity coupled Feed [21]

- **Aperture coupled feed**

This type of feed technique in figure 1.8, a microstrip feed line is separated by the ground plane to the radiating patch. The feed line and the radiating element is coupled through an aperture or a slot in the ground plane. The variations in the coupling will depend of width and length of the slot to improve the simulation result of bandwidths and return losses. The slot is usually centered under the radiating element [20].

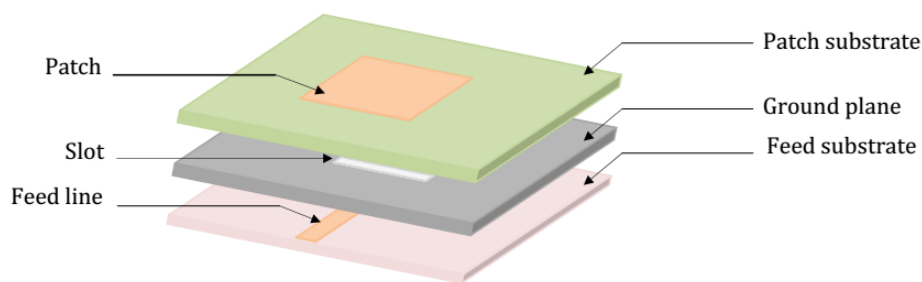


Figure 1. 8 Aperture coupled feed [21]

- **Coplanar Waveguide (CPW) feed**

In this technique the microstripæ line and the patch radiator and the ground plane are located on the same substrate as shown in figure 1.9 [20].

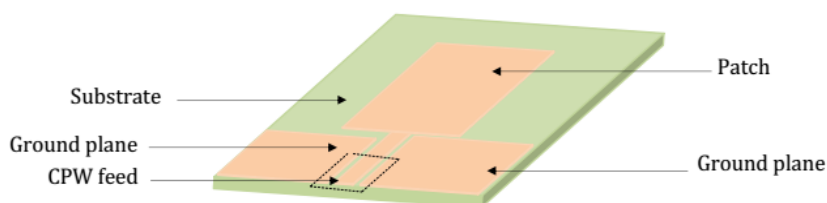


Figure 1. 9 Coplanar Waveguide (CPW) feed [21]

1.3.4 Fundamental antenna parameters

▪ Bandwidth

Bandwidth (BW) is the range of frequencies within which the performance of the antenna, with respect to some characteristic, conforms to a specified standard. The bandwidth can be considered to be the range of frequencies, on either side of the centre frequency, where the antenna characteristics are within an acceptable value of those at the centre frequency. Generally, in wireless communications, the antenna is required to provide a return loss less than -10 dB over its frequency bandwidth [22].

The frequency bandwidth of an antenna can be expressed as either absolute bandwidth (ABW) or fractional bandwidth (FBW). If f_H and f_L denote the upper edge and the lower edge of the antenna bandwidth, respectively. The ABW is defined as the difference of the two edges and the FBW is designated as the percentage of the frequency difference over the center frequency, as given in Equation (1.1) and (1.2), respectively.

$$\text{ABW} = f_H - f_L \quad (1.1)$$

$$\text{FBW} = \frac{f_H - f_L}{f_c} \quad (1.2)$$

For broadband antennas, the bandwidth can also be expressed as the ratio of the upper to the lower frequencies, where the antenna performance is acceptable, as shown in Equation (1.3).

$$\text{FBW} = \frac{f_H}{f_L} \quad (1.3)$$

▪ Radiation Pattern

The radiation pattern (or antenna pattern) is the representation of the radiation properties of the antenna as a function of space coordinates. In most cases, it is determined in the far-field region where the spatial (angular) distribution of the radiated power does not depend on the distance. Usually, the pattern describes the normalized field (power) values with respect to the maximum values .

The radiation property of most concern is the two- or three-dimensional (2D or 3D) spatial distribution of radiated energy as a function of the observer's position along a path or surface of constant radius. In practice, the three-dimensional pattern is sometimes

required and can be constructed in a series of two-dimensional patterns. For most practical applications, a few plots of the pattern as a function of φ for some particular values of frequency, plus a few plots as a function of frequency for some particular values of θ will provide most of the useful information needed, where φ and θ are the two axes in a spherical coordinate system.

For a linearly polarized antenna, its performance is often described in terms of its principle E plane and H-plane patterns. The E-plane is defined as the plane containing the electric-field vector and the direction of maximum radiation whilst the H-plane is defined as the plane containing the magnetic-field vector and the direction of maximum radiation [23]. There are three common radiation patterns that are used to describe an antenna's radiation property:

• **Isotropic:** A hypothetical lossless antenna having equal radiation in all directions. It is only applicable for an ideal antenna and is often taken as a reference for expressing the directive properties of actual antennas.

• **Directive:** An antenna having the property of radiating or receiving electromagnetic waves more effectively in some directions than in others. This is usually applicable to an antenna where its maximum directivity is significantly greater than that of a half-wave dipole.

• **Omni-Directional:** An antenna having an essentially non-directional pattern in a given plane and a directional pattern in any orthogonal plane.

▪ Directivity

To describe the directional properties of antenna radiation pattern, directivity D is introduced and it is defined as the ratio of the radiation intensity U in a given direction from the antenna over that of an isotropic source. For an isotropic source, the radiation intensity U_0 is equal to the total radiated power P_{rad} divided by 4π . So the directivity can be calculated by [22]:

$$D = \frac{U(\hat{r})}{U_0} = \frac{U(\hat{r})}{\frac{P_{rad}}{4\pi}} \quad (1.4)$$

If not specified, antenna directivity implies its maximum value, i.e. D_0 .

$$D_0 = \frac{U_{max}}{U_0} = \frac{U_{max}}{\frac{P_{rad}}{4\pi}} \quad (1.5)$$

- **Gain**

The antenna absolute gain according to is defines as the ratio of the intensity, in a given direction, to the radiation intensity that would be obtained if the power accepted by the antenna were radiated isotropically. Antenna gain G is closely related to the directivity, but it takes into account the radiation efficiency e_{rad} of the antenna as well as its directional properties, as given by [22]:

$$G = e_{rad} \times D \quad (1.6)$$

Similarly, the maximum gain G_0 is related the maximum directivity D_0 by:

$$G_0 = e_{rad} \times D_0 \quad (1.7)$$

- **VSWR**

VSWR stands for Voltage Standing Wave Ratio, and is also referred to as Standing Wave Ratio (SWR). VSWR is a function of the reflection coefficient, which describes the power reflected from the antenna. If the reflection coefficient is given by Γ , then VSWR is defined as [22]:

$$VSWR = \frac{1 + |\Gamma|}{1 - |\Gamma|} \quad (1.8)$$

The VSWR is always a real and positive number for antennas. The smaller the VSWR is, the better the antenna is matched to the transmission line and the more power is delivered to the antenna. The minimum VSWR is 1.0. In this case, no power is reflected from the antenna, which is ideal.

- **Beamwidth**

An antenna's beamwidth is usually understood to mean the half-power beamwidth. The peak radiation intensity is found, then the points on either side of the peak which represent half the power of the peak intensity are located. The angular distance between the half power points is defined as the beamwidth. Half the power expressed in decibels is -3dB, so the half power beamwidth is sometimes referred to as the 3dB beamwidth. Both horizontal and vertical beamwidths are usually considered.

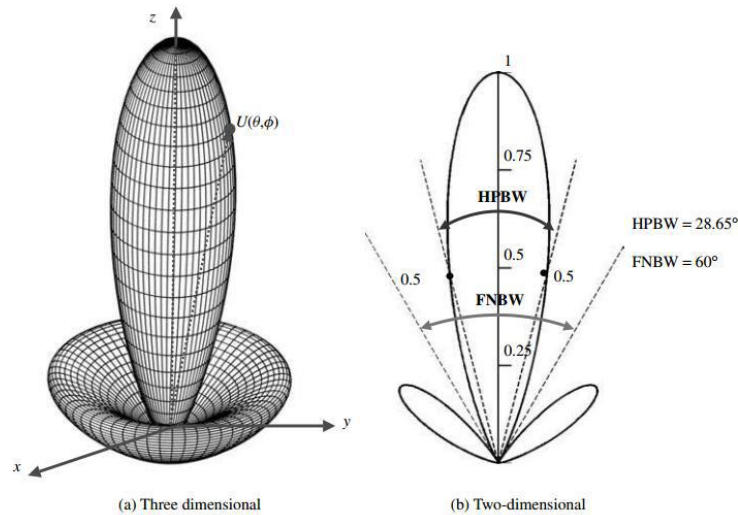


Figure 1.10 Three and two-dimensional power patterns [24]

Return Loss

The return loss represents the amount of power reflected by the antenna with respect to the incident power and is expressed with the following equation:

$$RL = -10 \log_{10} \left(\frac{P_r}{P_i} \right) \tag{1.9}$$

Where P_r is the reflected power and P_i is the input power supplied by the source, and it is also expressed as:

$$RL = -10 \log_{10} \left(\frac{Z_L - Z_0}{Z_L + Z_0} \right)^2 \tag{1.10}$$

Where Γ is the impedance matching between the characteristic impedance Z_0 and the load impedance Z_L . The reflection coefficient Γ is defined as:

$$\Gamma = \frac{Z_L - Z_0}{Z_L + Z_0} \tag{1.11}$$

The return loss should be less than -10 dB in the operating frequency band.

1.3.5 Methods of Analysis

There are many methods of analysis for microstrip antennas. The most popular models are:

- Transmission-line model.
- Cavity model.
- Method of moments.
- FDTD method.

- Finite Element method.

The transmission-line model is the easiest of all, it gives good physical insight, but is less accurate and it is more difficult to model coupling. Compared to the transmission-line model, the cavity model is more accurate but at the same time more complex. However, it also gives good physical insight and is rather difficult to model coupling, although it has been used successfully. In general when applied properly, the full-wave models (which include primarily integral equations/Moment Method) are very accurate, very versatile, and can treat single elements, finite and infinite arrays, stacked elements, arbitrary shaped elements, and coupling. However they are the most complex models and usually give less physical insight [15].

1.4 MIMO systems

Multiple-Input-Multiple-Output (MIMO) technology has attracted attention in modern wireless communication systems. A significant increase in channel capacity is achieved without the need of additional bandwidth or transmit power by deploying multiple antennas for transmission to achieve an array gain and diversity gain, thereby improving the spectral efficiency and reliability. MIMO antenna systems require high decoupling between antenna ports and a compact size for application in portable devices [25].

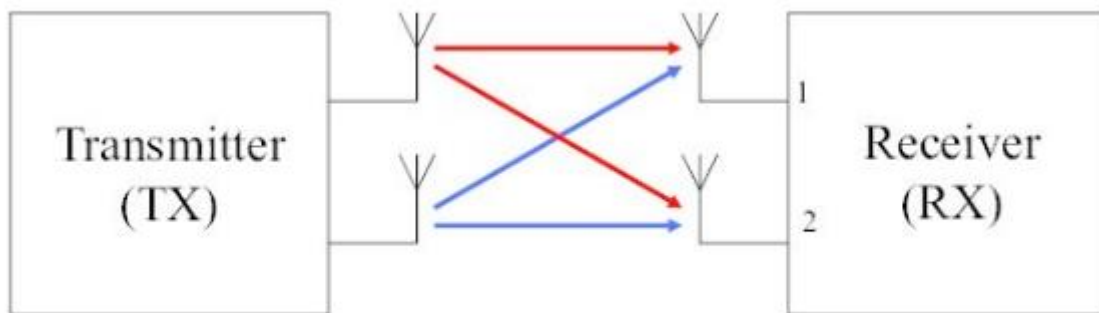


Figure 1. 11 MIMO 2x2 system, graphical representation [25]

Multiple-Input Multiple-Output (MIMO) uses multiple antennas on both the transmitter and receiver. They have dual capability of combining the SIMO and MISO technologies. They can also increase capacity by using Spatial multiplexing (SM). The MIMO method has some clear advantages over Single-input Single-output (SISO) methods. The fading is greatly eliminated by spatial diversity; low power is required compared to other techniques in MIMO [26].

The basic building blocks of a MIMO system are shown in the figure 1.12. In this figure, x and y represent the transmitted and received signal vectors respectively. At first, the information to be transmitted is encoded and interleaved. The symbol mapper maps the encoded information to data symbols. These data symbols are then fed into a space-time encoder which creates some spatial data streams. The data streams are then transmitted by different antennas. The transmitted signals are propagated through channels and are received by receiving arrays. The receiver then collects all the data from the antennas and reverses the operation to decode the data using a space-time processor, space time decoder, symbol demapper and at last the decoder [27].

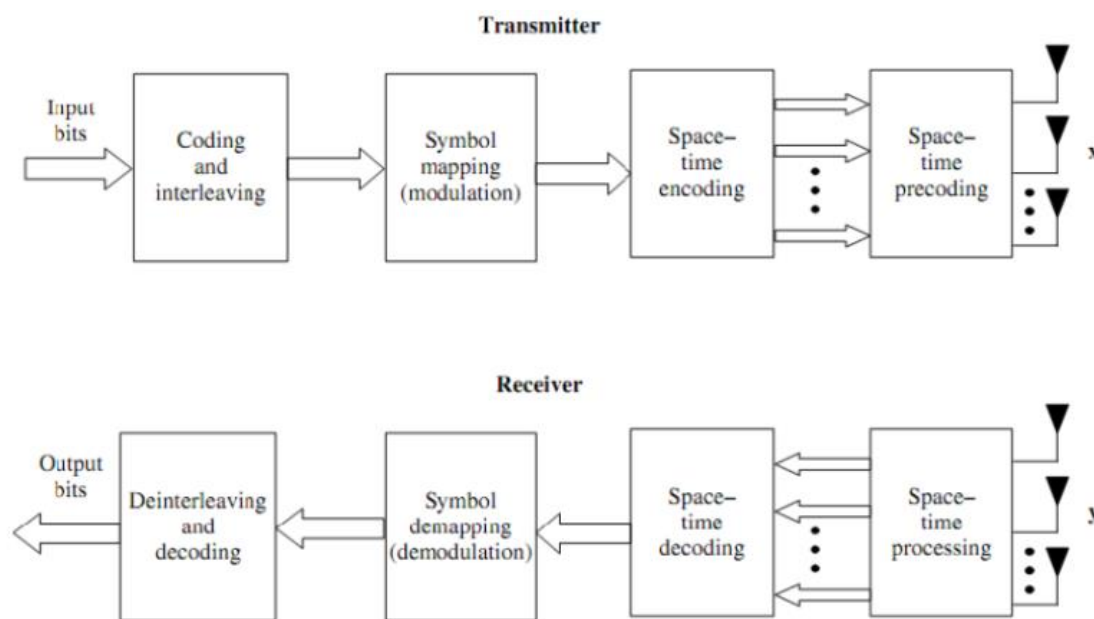


Figure 1. 12 Building Blocks of a MIMO system [28]

Initially, MIMO systems focused on basic spatial diversity (the MIMO system technology was used to attenuate the degradation caused by multipath propagation). However, this technology started to use the multipath propagation as an advantage, turning the additional signal paths into what might effectively be considered as additional channels to carry additional data [29-30].

Using a multiple number of antennas, with MIMO wireless technology systems it is possible to transmit data with a substantial growth of the channels capacity without contravening Shannon's law [31].

1.4.1 MIMO antennas special parameters

Significant SNR improvement and added gain is expected when using diversity systems, which are evaluated by three main parameters: correlation coefficient, diversity gain and antenna efficiency (that is not included in this work).

▪ Signal port correlation coefficient

The correlation coefficient is the relationship between the incoming signals at the antenna ports in an array. Mutual coupling in array systems degrades the performance of the array. The correlation coefficient between antennas is used as a performance metric in multiple-input multiple-output (MIMO) systems to quantify the system performance and efficiency of the antennas. By using the correlation coefficient, a MIMO system designer is able to understand the level of coupling that exists between the antenna ports in the system. To minimize the mutual coupling would imply to reduce the correlation coefficient the lowest possible between the pairs of ports. Correlation coefficient is calculated using S-parameter by using [32]:

$$\rho_{ij} = \frac{S_{ij} - S_{ji}}{S_{ii} - S_{jj}} \quad (1.12)$$

▪ Diversity gain

Diversity gain is an advantage that is used to quantify the performance of diversity techniques. It is a slope of the error probability curve in terms of the received SNR in a log-log scale. A good diversity gain leads to a good SNR relationship. To measure this coefficient, it is necessary to consider the total radiation efficiency and the correlation coefficient as described in the following equation [33]:

$$D_g = \frac{1}{\rho} \quad (1.13)$$

A good isolation between antenna's elements requires the higher value of the diversity gain.

1.5 Conclusion

A review about antenna parameters, microstrip antennas as well as smart grids has been given throughout this chapter. It has been observed that different frequency bands are used in smart grids wireless communication systems among which the WiMAX bands around 3.5 and 5.8 GHz and Wi-Fi bands around 5.6 GHz in which the developed MIMO antennas operate.

Ultra Wide Band MIMO Antenna

2.1 Introduction

The aim of this chapter is the design of an UWB antenna that covers WiMAX frequencies 3.5 and 5.8 GHz that are used in smart grids networks.

The procedure starts by considering a single element antenna. A parametric analysis as well as slots insertion has been performed to improve the structure performance related to the operating bandwidth.

A two-element MIMO structure is then considered in order to study isolation between the ports with different orientations.

Finally, the best orientation is used to design a four-element MIMO antenna.

2.2 Geometry and simulation of reference element

2.2.1 Basic antenna Structure

A microstrip-fed Printed Circular Disc Monopole (PCDM) antenna is designed on the FR4 substrate of thickness of 1.6 mm, relative permittivity of 4.4 and tangent loss of 0.02. The antenna consists of a circular disc radiator with a radius of 9.5 cm connected to a microstrip line feed by 50-ohm SMA connector on the down side of the substrate and a partial ground plane compound by rectangle and half of an ellipse on the bottom side, as shown in figure 2.1.

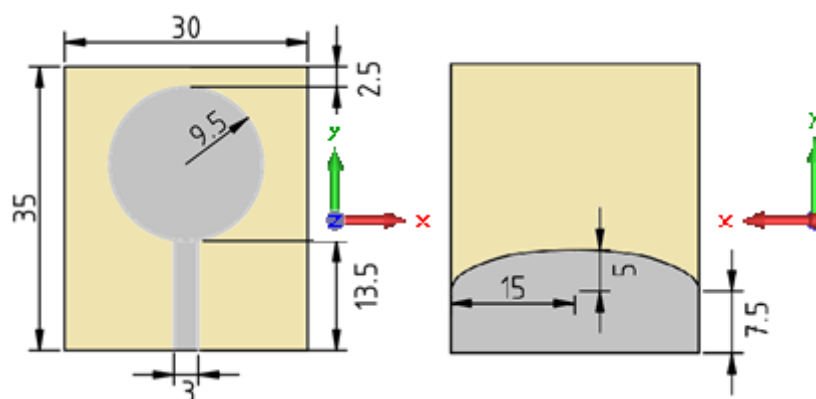


Figure 2. 1 Circular microstrip UWB antenna

The results are simulated using CST Microwave Studio 2015 package. Figure 2.2 shows the reflection coefficient versus frequency.

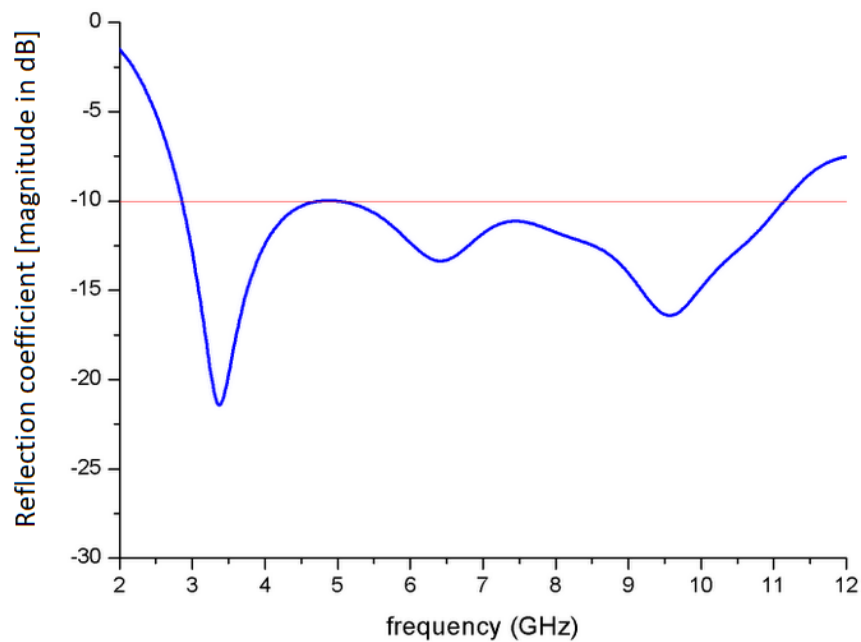


Figure 2. 2 Reflection coefficient of the basic UWB antenna

It is observed from the graph that the operating frequencies of the antenna are between 2.85 GHz and 11.5 GHz, therefore the antenna is considered as an UWB antenna as it includes the band 3.1 -10.6 GHz characterizing such structures.

2.2.2 Antenna improvement and optimization

First, a rectangular slot of dimension of 4.2×3 mm² is inserted on the ground plane as shown in figure 2.3. The dimensions of the slot were selected after doing parametric studies about the effects of the width and the length on the reflection coefficient.

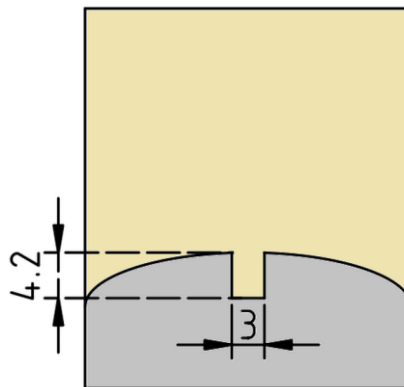


Figure 2. 3 Slotted Ground plane of the antenna

The effect of inserting a rectangular slot on the ground plane on the reflection coefficient is illustrated in figure 2.4.

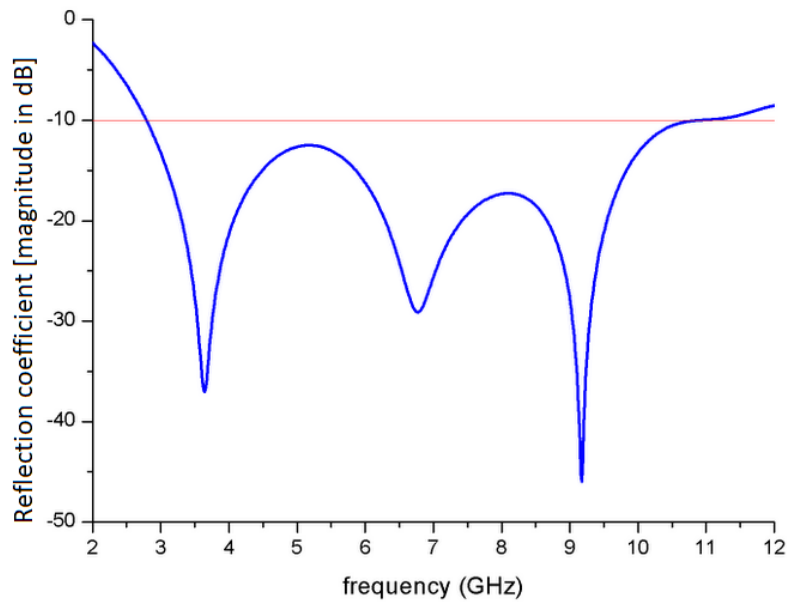


Figure 2. 4 Reflection coefficient of the antenna with a slotted ground

We notice from this figure that the reflection coefficient is enhanced especially at higher frequencies which have a return loss less than -15 dB and almost no change is introduced to the bandwidth.

In the following modification, two square slots (stubs) of 1 mm^2 are inserted on the bottom of the circular patch as illustrated in figure 2.5

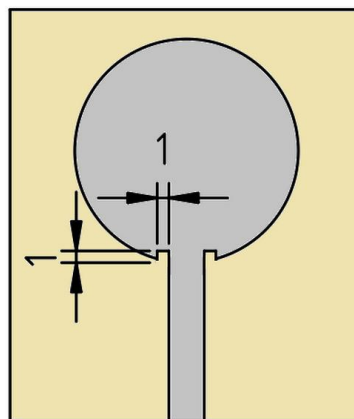


Figure 2. 5 Antenna structure after adding square slots

The corresponding reflection coefficient is shown in figure 2.6.

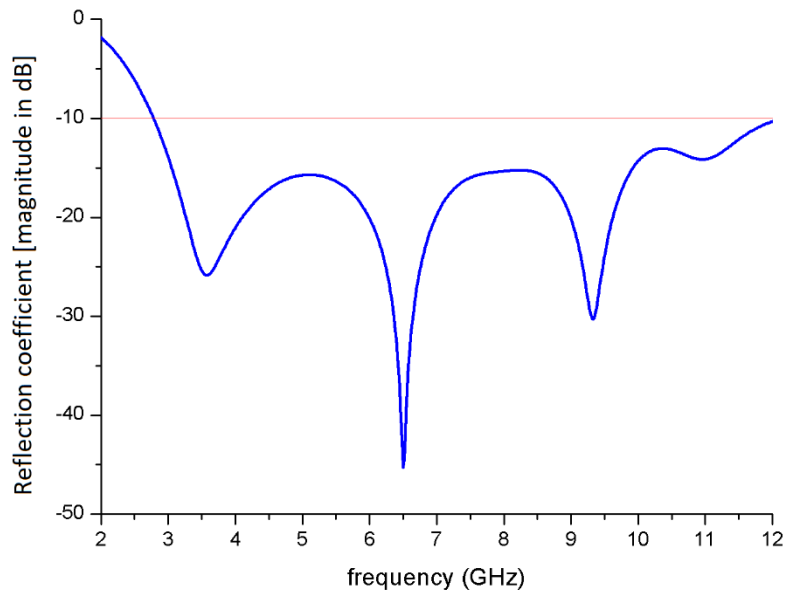


Figure 2. 6 Reflection coefficient of the slotted patch antenna

The reflection coefficient is less than -15 dB for large frequency intervals and the higher frequency band limit increases to 12.23 GHz.

Finally, the patch is cut from the upper side as illustrated in figure 2.7. The length 5.5 mm was selected after parametric study.

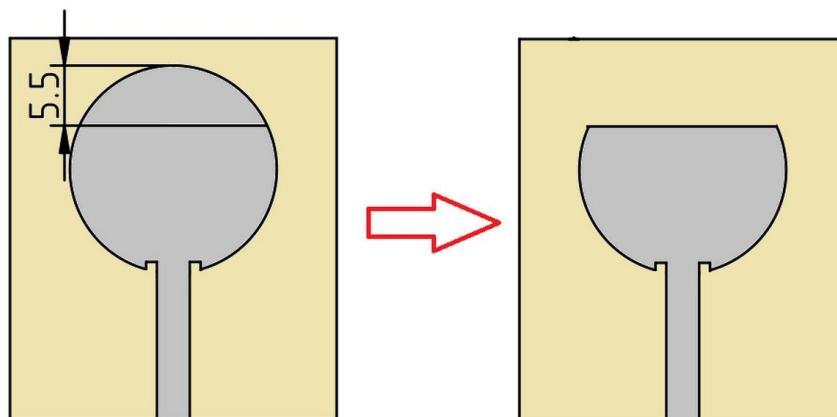


Figure 2. 7 Final antenna structure

Figure 2.8 shows the final antenna reflection coefficient where we notice that the lower frequency moves to 3.11 GHz and S_{11} has better matching compared to the previous structures. The final structure is considered as the reference antenna.

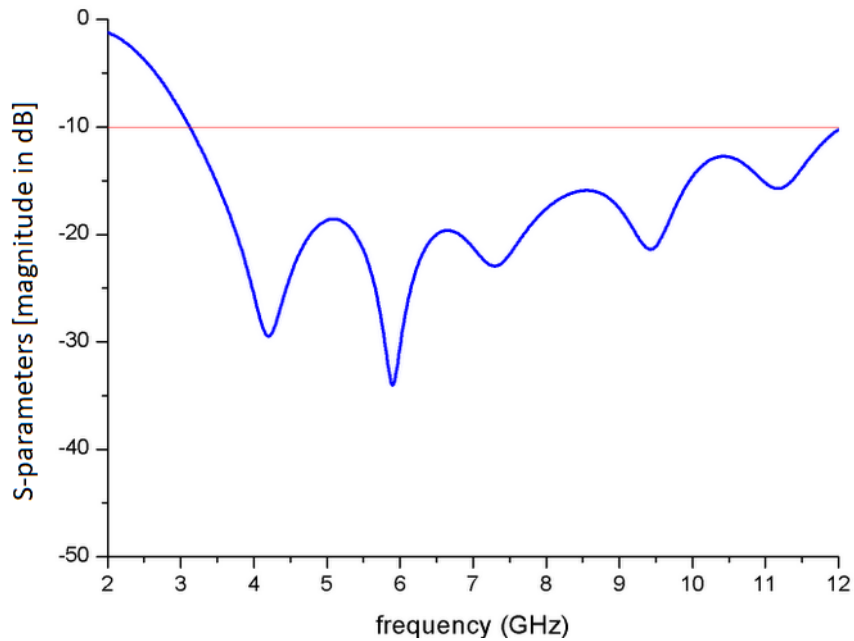


Figure 2. 8 Reflection coefficient of the reference UWB antenna

Figure 2.9 represents the antenna gain versus frequency. The gain increases with the frequency from 2 GHz to reach a maximum of 4.47 dBi at 8 GHz. At the remaining frequency interval within the bandwidth, the gain is quite constant.

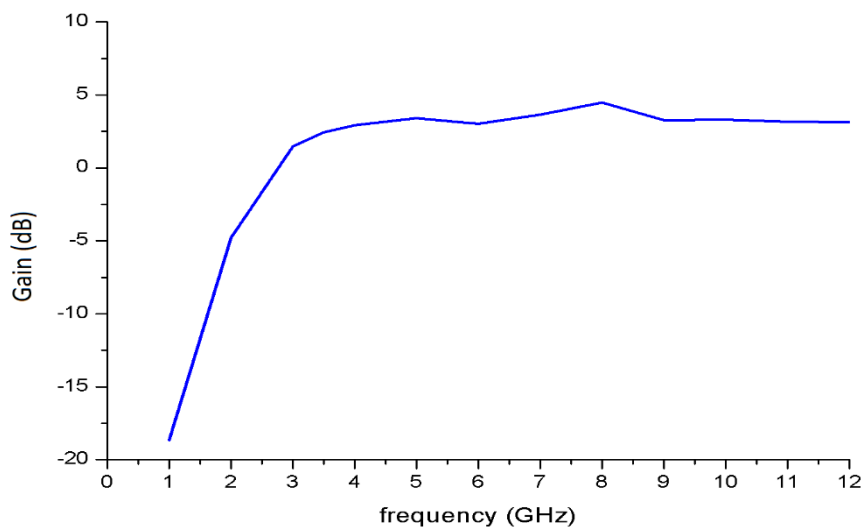


Figure 2. 9 Simulated gain vs. frequency of the reference UWB antenna

Figure 2.10 shows the surface current distribution at WiMAX frequencies (3.5 GHz and 5.8 GHz). It is seen that the current density is high on the feed line and on the outer edge of the disc patch for the frequency 3.5 GHz. However, for the frequency 5.8 GHz, a significantly higher density is observed on the feed line.

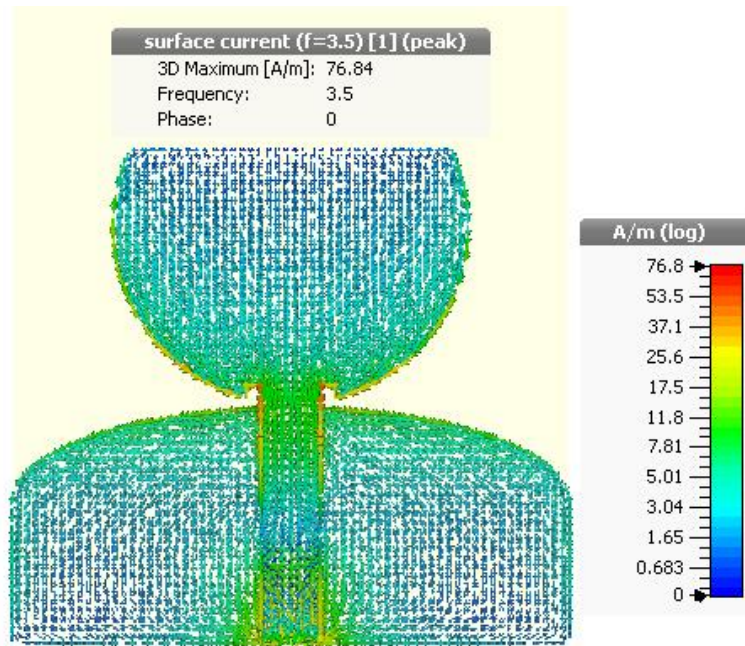
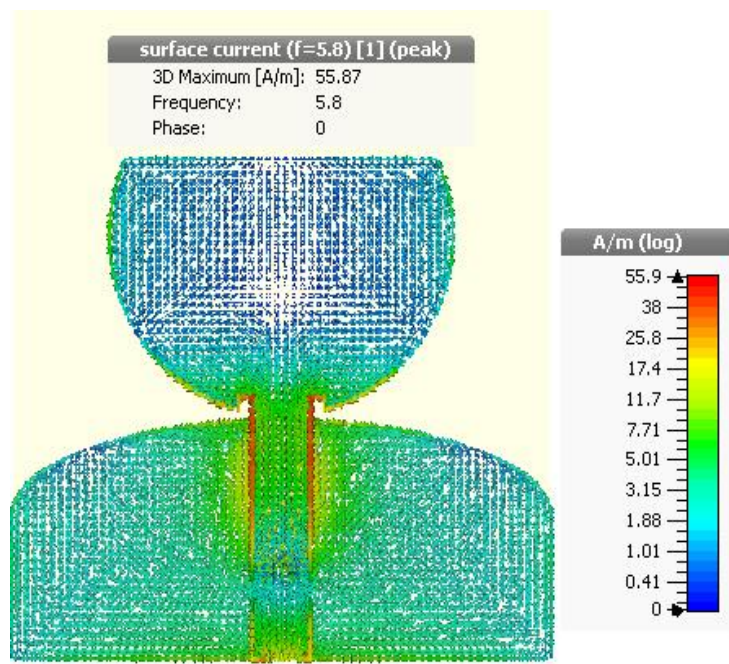
(a) $f = 3.5$ GHz(b) $f = 5.8$ GHz

Figure 2. 10 Surface current distribution of the reference UWB antenna

Figures 2.11 and 2.12 illustrate the 3-D and the 2-D radiation patterns at the frequencies 3.5 and 5.8 GHz in the principle planes.

Figure 2.12 shows that at the frequency 3.5 GHz the pattern is almost omnidirectional in the plane $\varphi = 0^\circ$ and presents two lobes, in the lower and the upper sides of the patch, in the plane

$\phi = 90^\circ$. However, at the frequency 5.8 GHz the radiation pattern is illustrated by two main lobes in both planes.

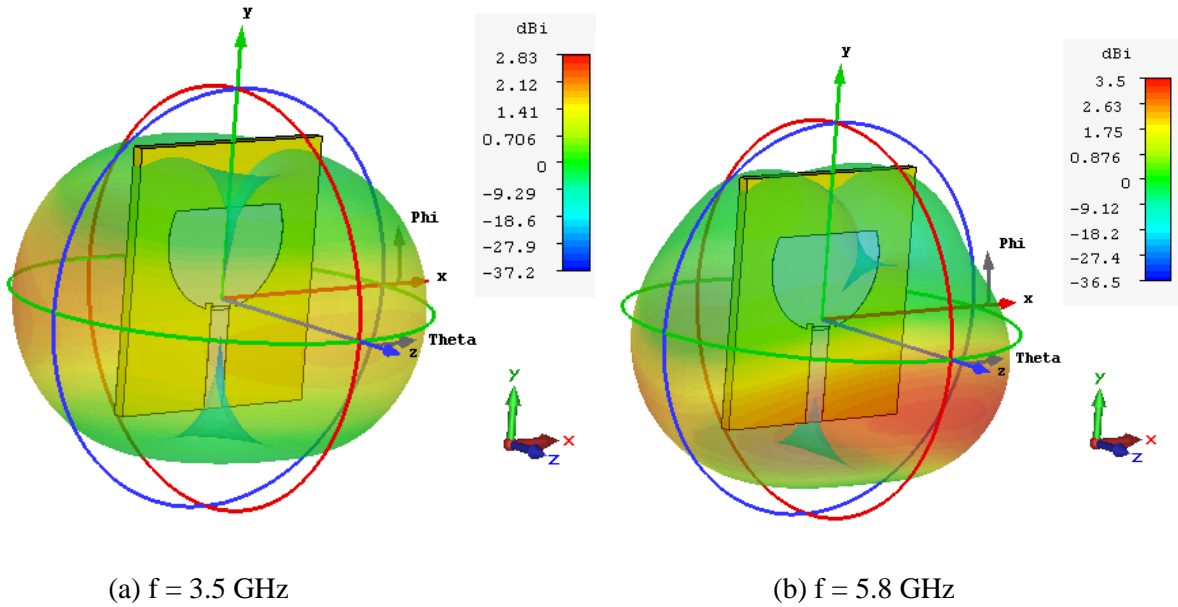


Figure 2. 11 3-D Radiation pattern of the reference UWB antenna

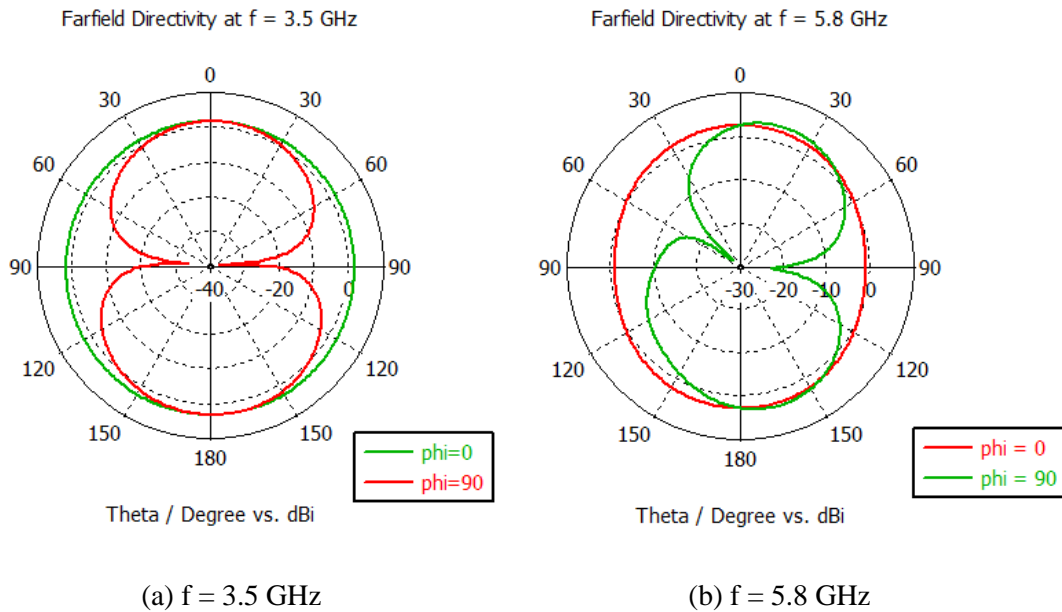


Figure 2. 12 2-D Radiation pattern for 3.5 and 5.8 GHz of the reference UWB antenna

2.3 Design and simulation of two-element MIMO antenna

This section presents MIMO configurations composed of two-reference antennas discussed in the previous section and studies the isolation between the two elements in each configuration. Antenna to antenna isolation is a measure of how tightly coupled antennas are. Typically, the isolation should be as large as possible. The method of measuring isolation is typically done by connecting both antennas to a Vector Network Analyzer, and measuring S_{12} (S_{21}) parameter. This measured parameter should be less than -15 dB in order to get a good isolation.

Antenna to antenna isolation can be increased by:

- x Increasing the physical separation between the antennas (not very practical).
- x Using different polarizations for the antennas (Antenna placement and orientation).

In the first configuration, the structure is composed of two reference antennas that are side by side (spatial diversity) with a narrow spacing of $d=0.5$ mm between them in order to separate the ground plane of each antenna as shown in figure 2.13.

“Port 1” refers to the element displayed on the left and “Port 2” the other one for all two-element antenna proposed in this section.

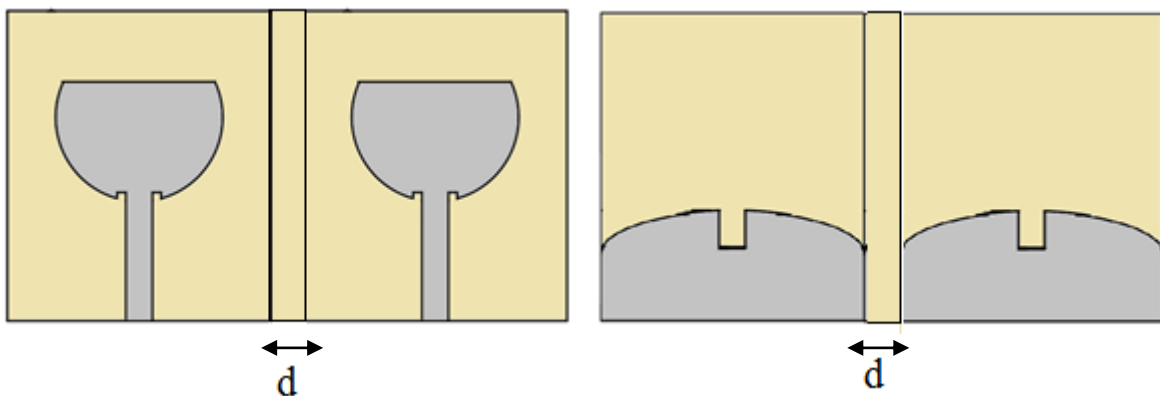


Figure 2. 13: Two parallel UWB antenna configuration.

From the S-parameters presented in figure 2.14, it is observed that $S_{11} = S_{22}$ and $S_{12} = S_{21}$ because of the axial symmetry between the two antennas. From S_{12} and S_{21} curves, the mutual uncoupling between ports 1 and 2 is present in a large range of frequencies except at low frequencies where it is comparatively high.

Moreover, figures 2.15-16 show acceptable correlation coefficient and diversity gain between ports.

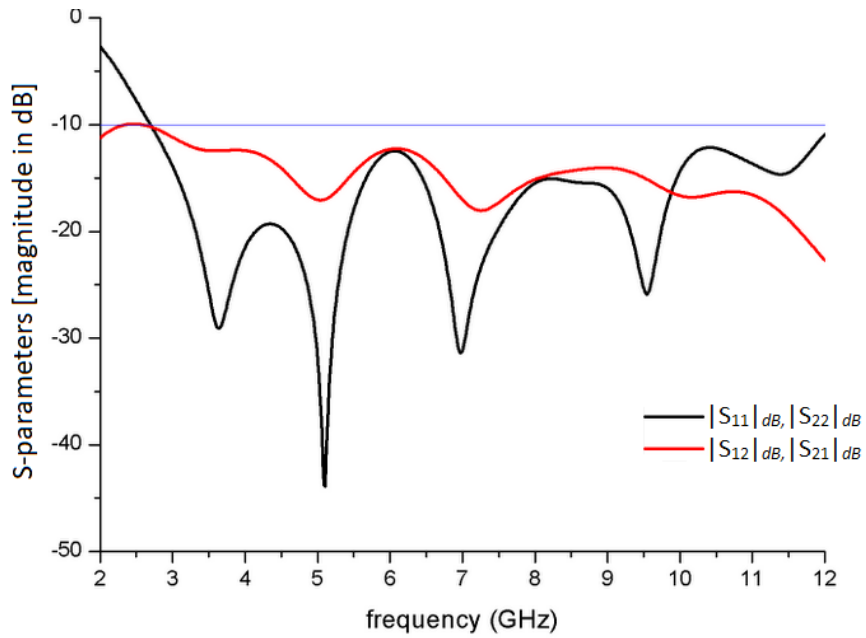


Figure 2. 14 S-parameters of two parallel UWB antennas

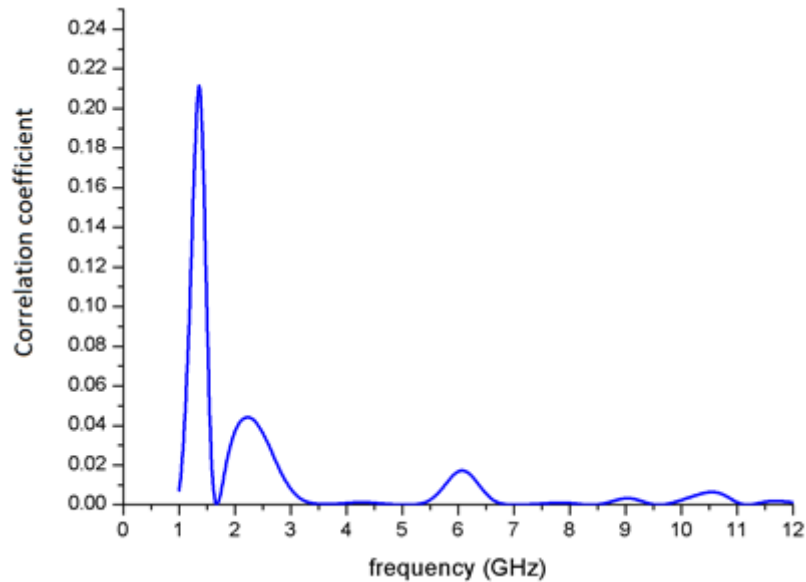


Figure 2. 15 Correlation coefficient of two parallel UWB antennas

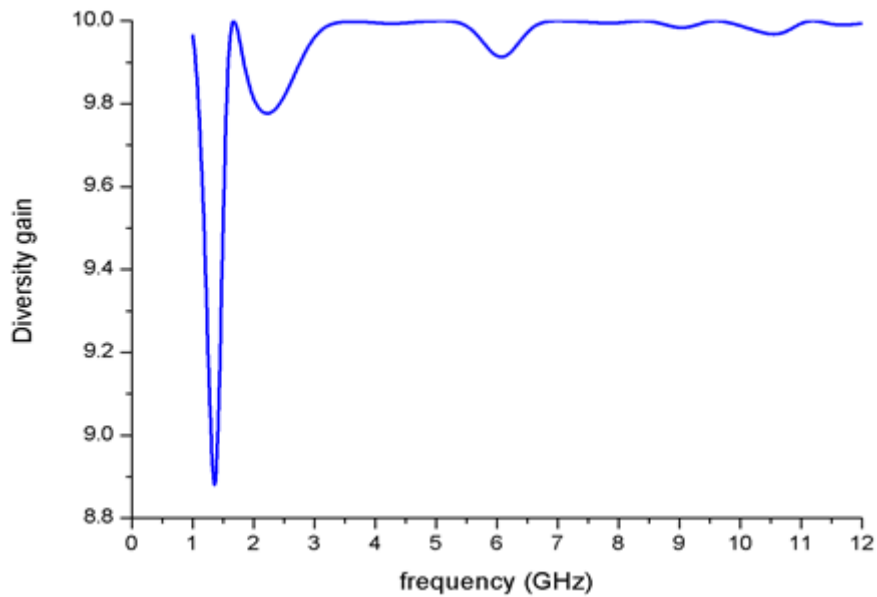


Figure 2. 16 Diversity gain of two parallel UWB antennas

In the next structure, the distance of separation between the two side by side antennas is increased to $d=10$ mm.

Figure 2.17 illustrates the new S-parameters. It is noticed that the isolation is improved compared to the previous configuration but it is still relatively high at low frequencies.

For the ports correlation coefficient all peak values decrease and increase for diversity gain.

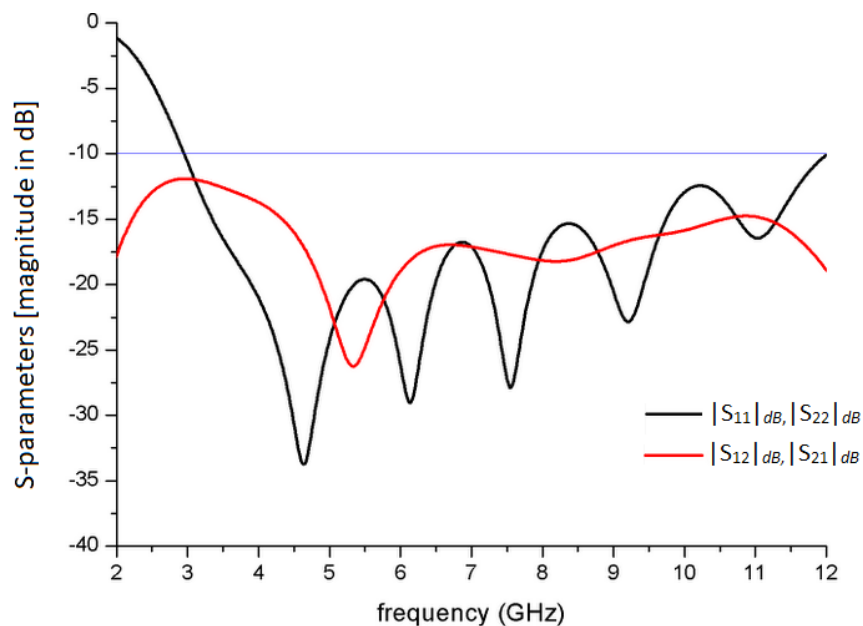


Figure 2. 17 S-parameters of two parallel UWB antennas with a spacing of 10 mm

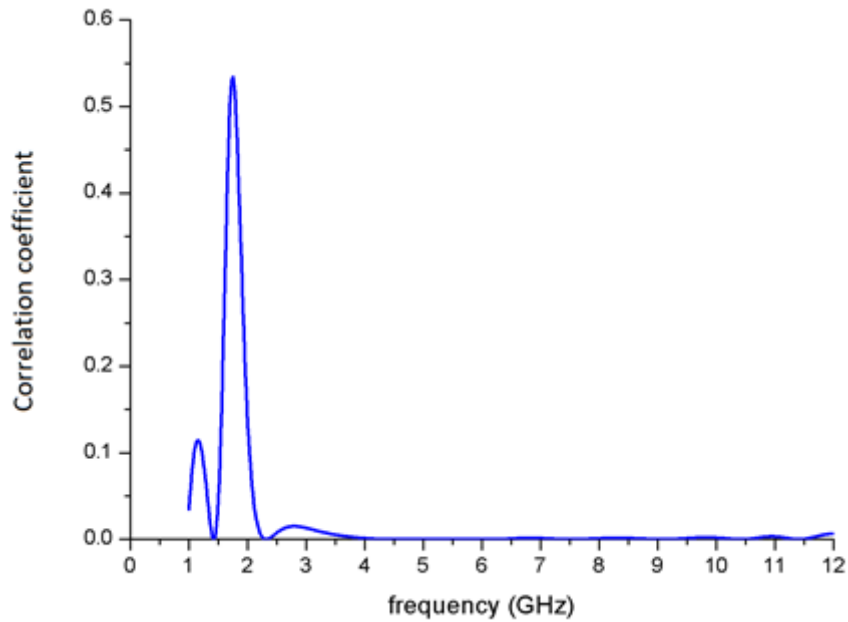


Figure 2. 18 Correlation coefficient of two parallel UWB antennas with a spacing of 10 mm

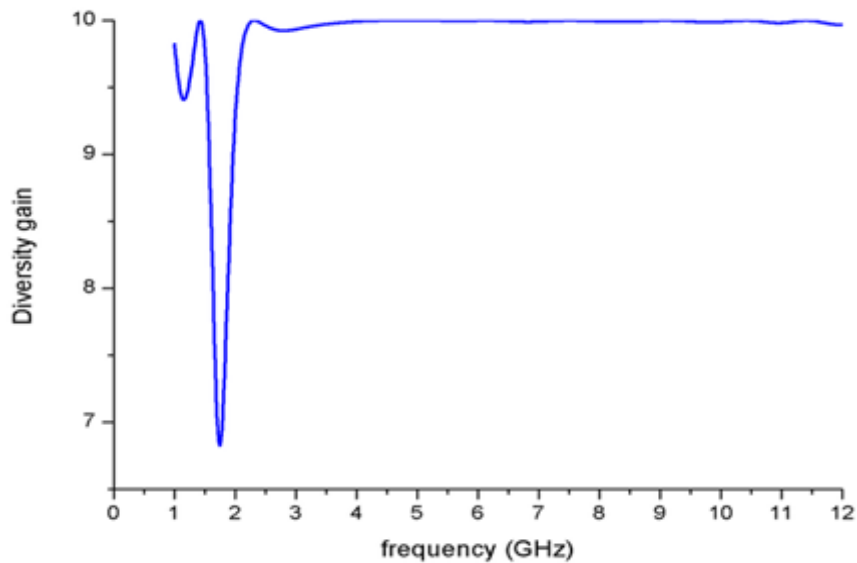


Figure 2. 19 Diversity gain of two parallel UWB antennas with a spacing of 10 mm

In this configuration, the two antennas are placed orthogonally (polarization diversity). The element on the left side is placed vertically while the other is placed horizontally as shown in figure 2.20. The right side of the figure (bottom view) showing the ground plane is obtained when flipping the up view figure.

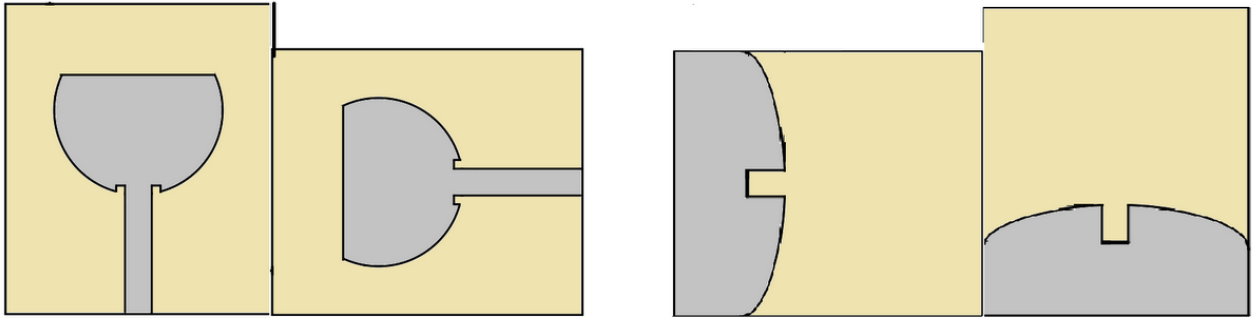


Figure 2. 20 Two orthogonal UWB antenna configuration

Observing figure 2.21, it concluded that the two antennas are totally isolated and uncoupled since S_{12} and S_{21} are less than -15 dB in the whole band.

The port correlation coefficient is approximately zero. The diversity gain takes values near to 10 in the required band of frequencies. Consequently, the antenna performances are improved with this configuration.

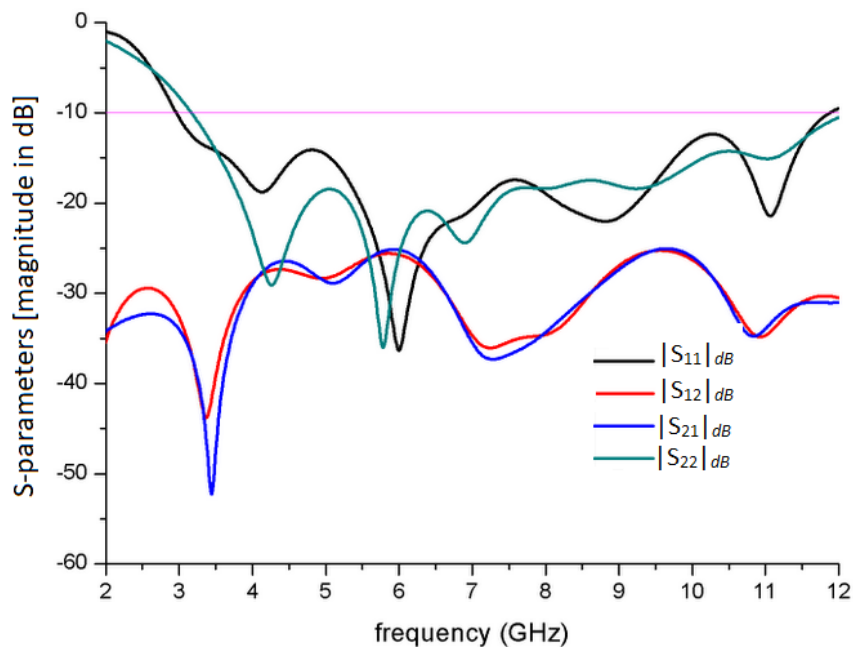


Figure 2. 21 S-parameters of two orthogonal UWB antennas

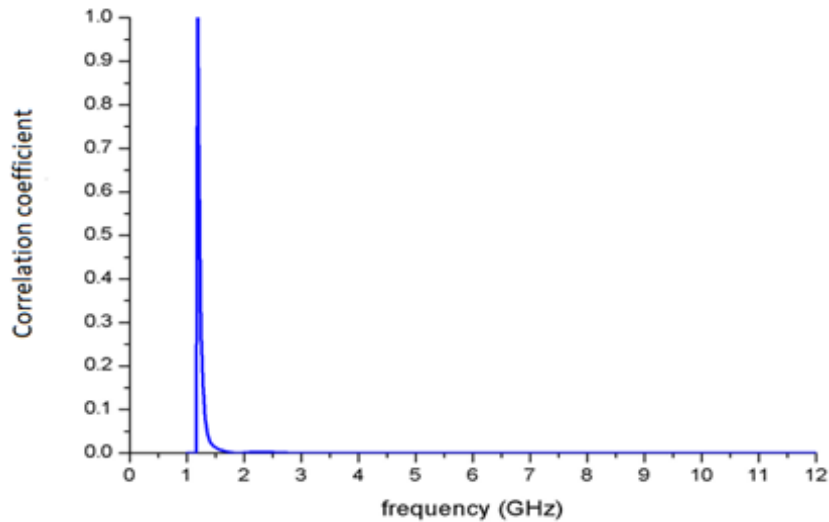


Figure 2. 22 Correlation coefficient of two orthogonal UWB antennas

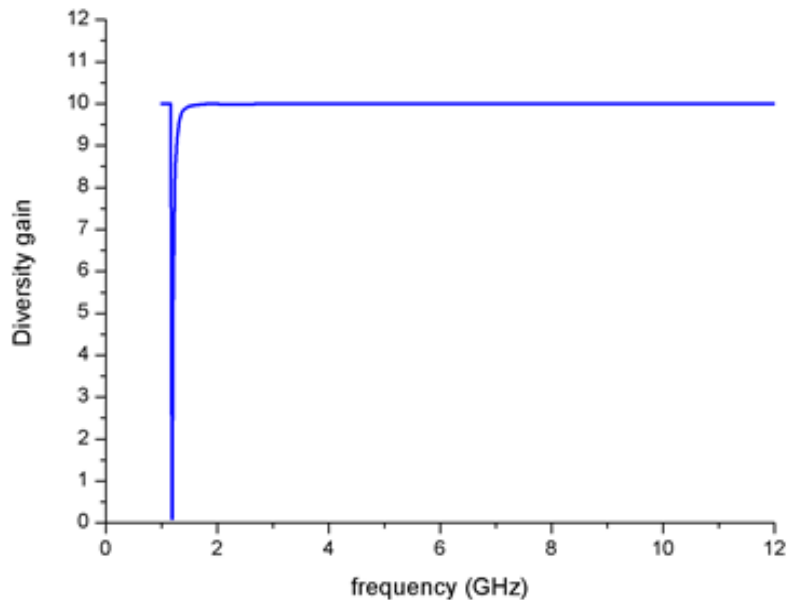


Figure 2. 23 Diversity gain for two orthogonal UWB antennas

From the above results, it is noticed that the orthogonal configuration provides the best results in terms of isolation, correlation coefficients and diversity gain.

2.4 Design and simulation of a four-element MIMO antenna

The configuration considered in this section has four elements arranged orthogonally as shown in figure 2.24. Since a single antenna is rectangular, a squared substrate of $5 \times 5 \text{ mm}^2$ is added at the center in order to fill the resulting space. Therefore, the total size of the antenna becomes $6.5 \times 6.5 \text{ mm}^2$.

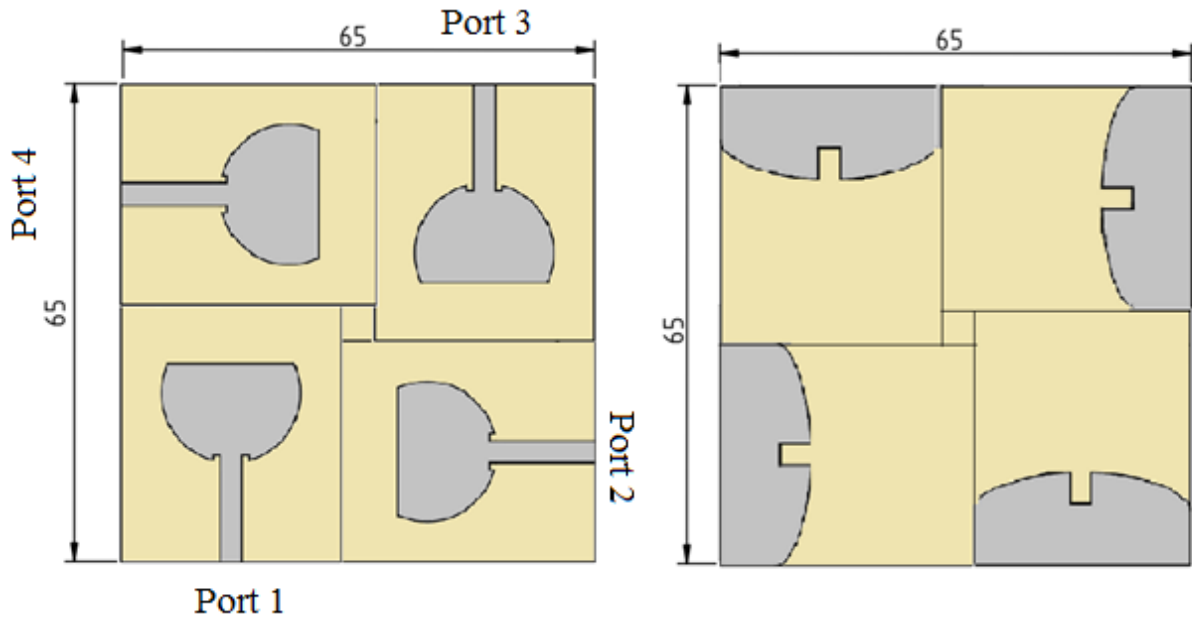


Figure 2. 24 Configuration of the 4-element UWB MIMO antenna

The proposed structure is symmetrical. Thus, all S_{ii} parameters have the same behavior over frequency. The parameters of adjacent port have the same behavior. By the same way, the ports, which arranged obliquely also, have the same behavior. Hence, it is concluded that there are only three curves of S-parameters as illustrated in the figure below.

These properties are expressed as:

- x $S_{11} = S_{22} = S_{33} = S_{44}$.
- x $S_{12} = S_{21} = S_{23} = S_{32} = S_{34} = S_{43} = S_{41} = S_{14}$.
- x $S_{13} = S_{31} = S_{24} = S_{42}$.

Hence, only three S-parameters indicated by each of the above equations are sufficient to describe the S-parameters of the 4-element MIMO configuration.

From figure 2.25, it is noted that:

- x The operating band of frequencies is from 3.15 to 11.7 GHz.
- x All elements are well isolated since all $|S_{ij}|_{i \neq j}$ values are under -15 dB

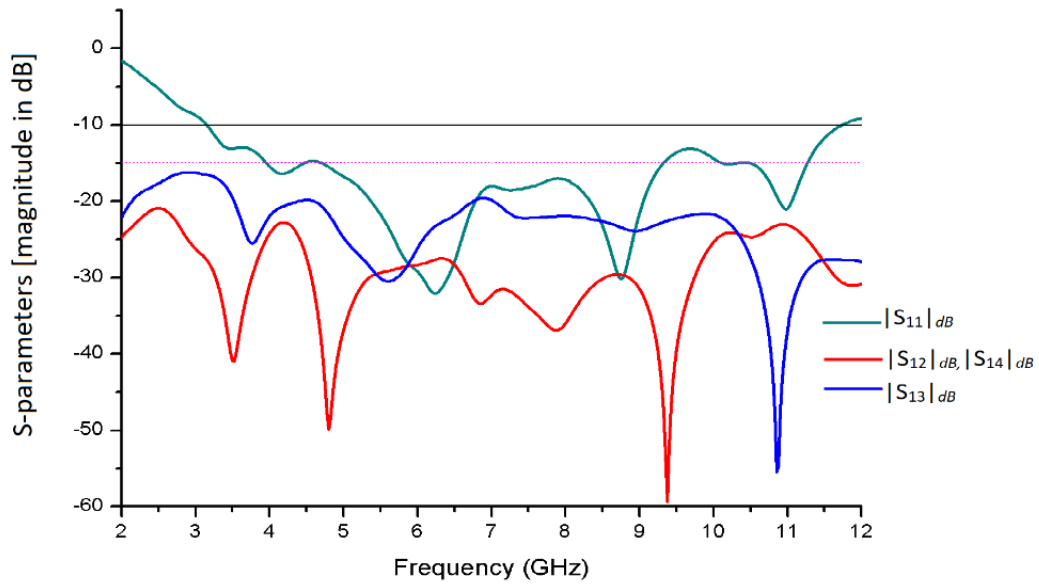


Figure 2. 25 S-parameters of UWB MIMO antenna at “port 1”

Figure 2.26 represents the 4-element UWB antenna gain versus frequency. It is shown that gain is enhanced to reach a maximum of 6.1 dBi at 8 GHz in contrast of 4.47 dBi at the same frequency for the reference antenna.

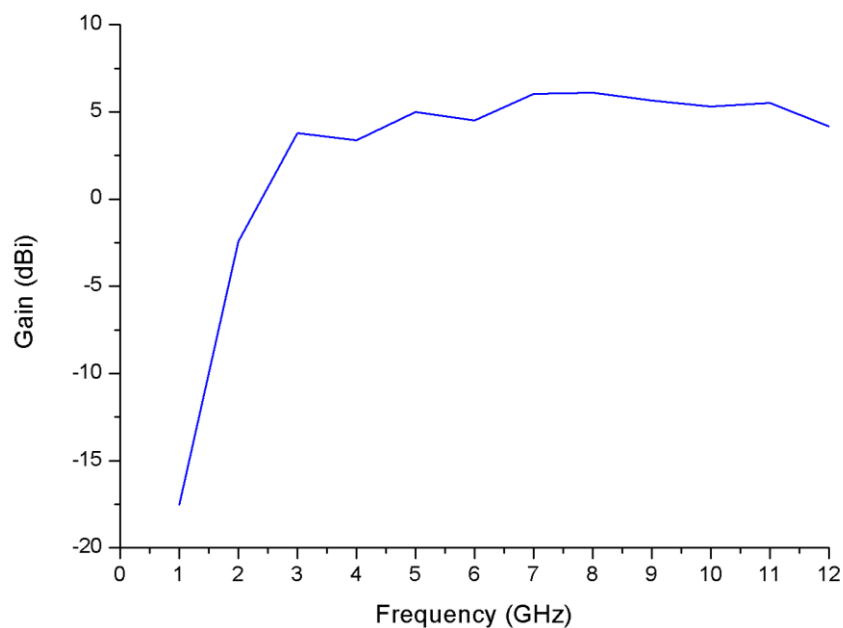


Figure 2. 26 Simulated gain vs. frequency of the 4-element UWB MIMO antenna

Because of symmetry, adjacent ports have the same port correlation and diversity gain curves and, this is similar for oblique ports as shown in figures 2.27-30.

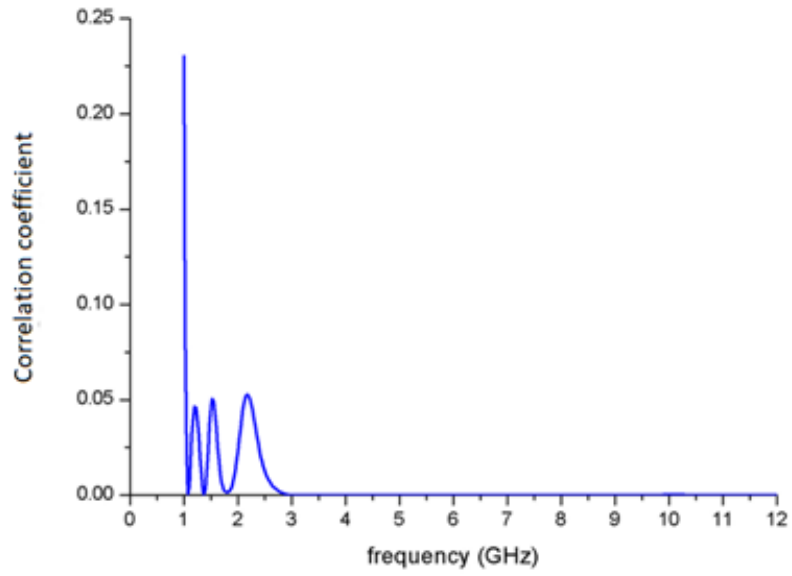


Figure 2. 27 Correlation coefficient between adjacent ports

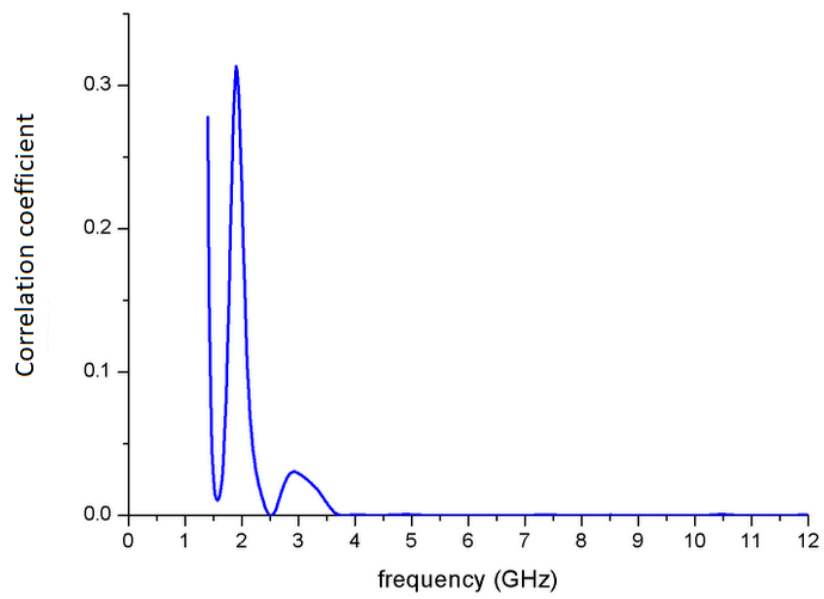


Figure 2. 28 Correlation coefficient between oblique ports

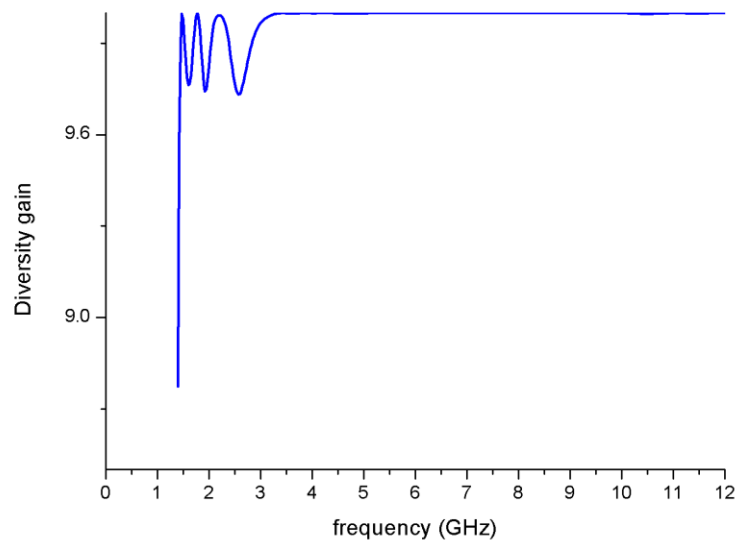


Figure 2. 29 Diversity Gain between adjacent ports

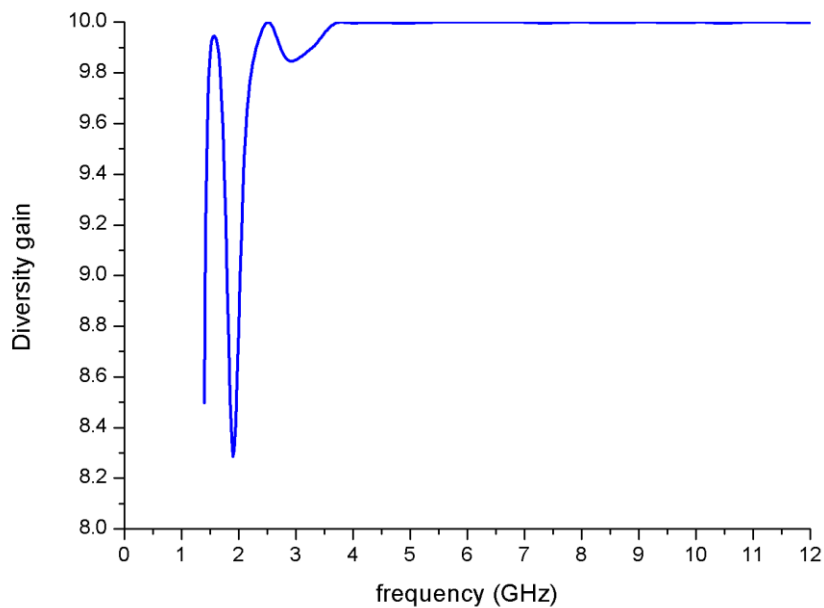


Figure 2. 30 Diversity gain between oblique ports

From the above figures, it is observed that the envelope correlation coefficient is very low at the desired frequency band (close to zero), and diversity gain is greater than 9.8 (close to the maximum) which indicates the good isolation between the two elements.

The surface current distributions on the four elements by exciting “port 1” at frequencies 3.5 and 5.8 GHz are illustrated in figure 2.31 where we observe that the induced current in the

other elements is weak. The small induced current at 3.5 GHz in the oblique element “3” is explained by same polarization between element “1” and “3”. This indicated by the S_{13} coefficient in figure 2.25, which is relatively higher than the others.

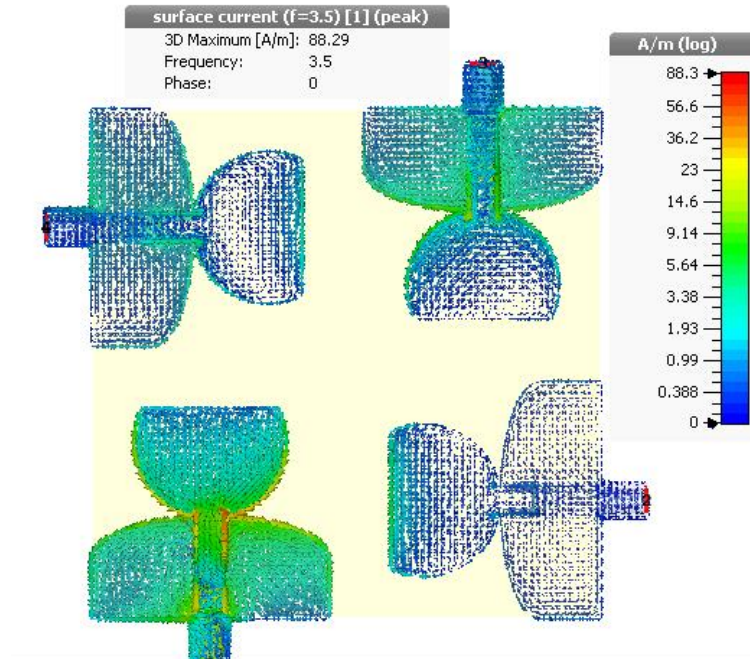
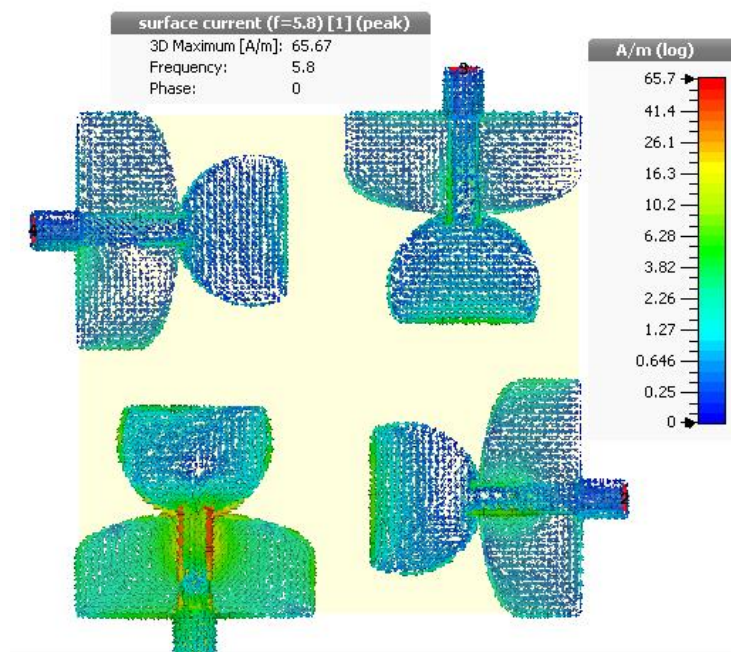
(a) $f = 3.5$ GHz(b) $f = 5.8$ GHz

Figure 2. 31 Surface current distribution of the 4-element UWB antenna

Figures 2.32 and 2.33 illustrate the 3-D and, the 2-D radiation patterns of the 4-element MIMO antenna by exciting “port 1” at the frequencies 3.5 and 5.8 GHz in the principle planes.

Figure 2.33 shows that the pattern presents three lobes in the plane $\phi = 0^\circ$ and two lobes in the plane $\phi = 90^\circ$ for both frequencies with equivalent directivity in each plane.

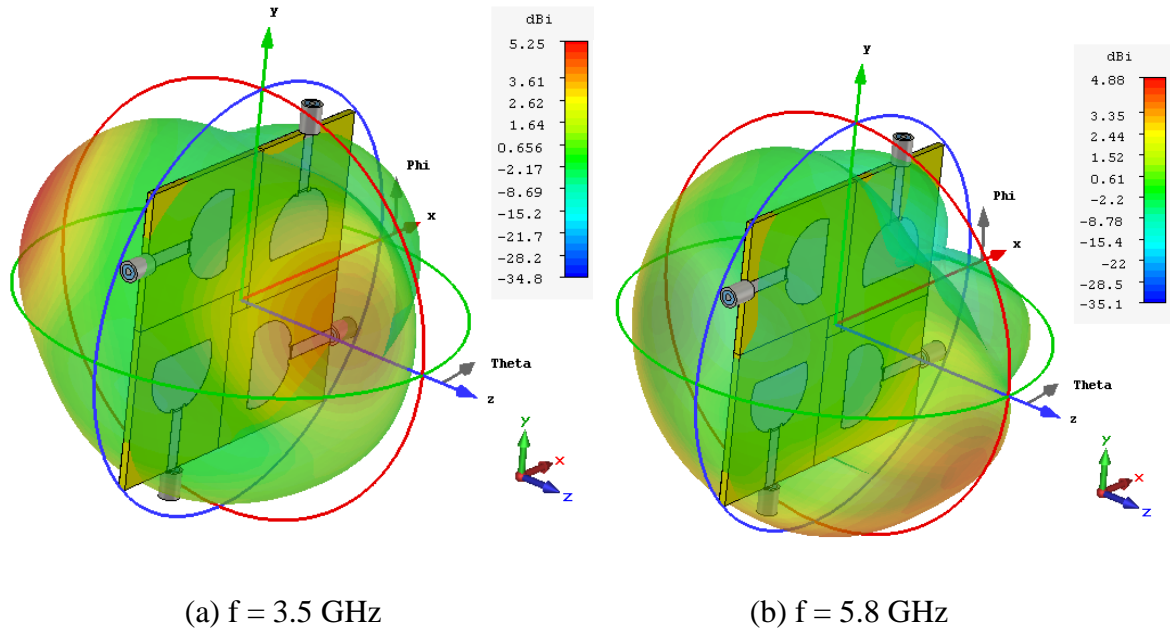


Figure 2. 32 3-D radiation pattern of the UWB MIMO antenna

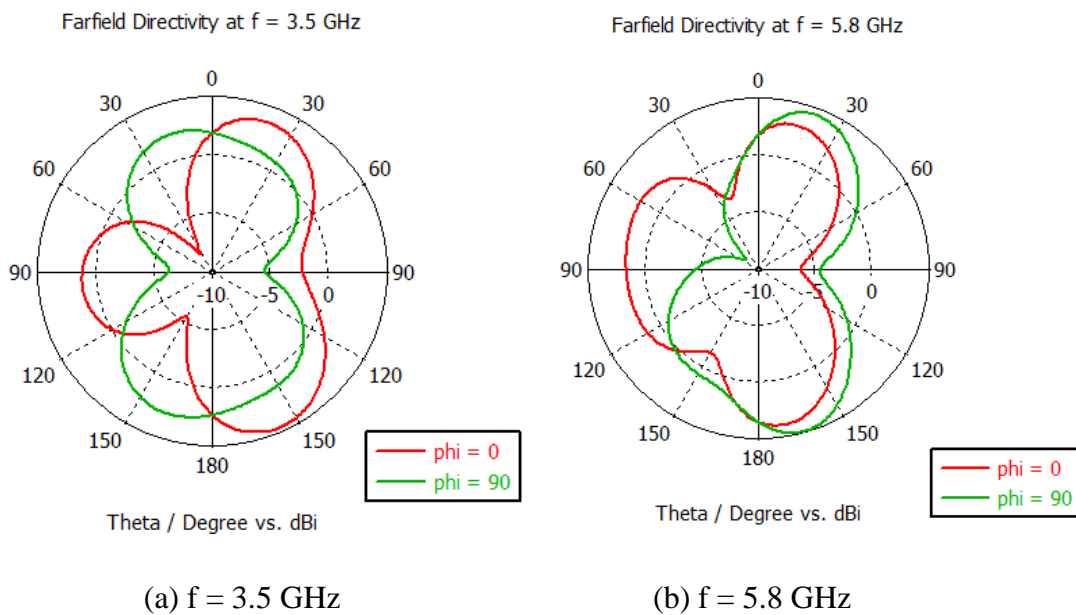


Figure 2. 33 2D radiation pattern at different frequencies when exciting “port 1”

2.5 MIMO antenna system prototypes measurements

The fabrication process of the desired 2×2 MIMO antenna was done in SNC ALMITech enterprise laboratory in Kouba (Algiers).

Many steps are needed to produce a printed antenna, which are:

- x The mask of the antenna was exported from CST Microwave studio ® in format of Gerber file.
- x A photographic film was printed to minimize precision errors.
- x The FR4 epoxy glass was chosen as a substrate material.
- x The circuit is printed based on photographic film by transferring the geometry of a mask to a surface, this process is done by illuminating the copper by ultra-violet radiation. The copper, which is not illuminated, is removed using various chemicals that are called photo resists, which are organic polymers that change its chemical characteristics when exposed to ultraviolet light.
- x The obtained antenna is shown in figure 2.34.

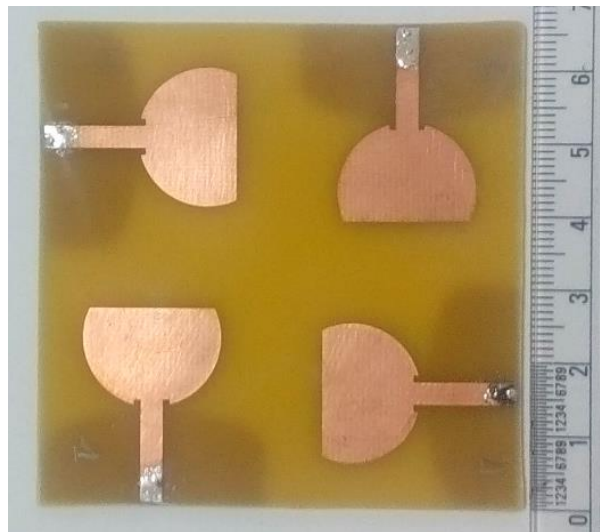


Figure 2. 34 Manufactured UWB 2×2 UWB MIMO antenna

- x Four SMA connectors (50-ohm impedance) were welded to each feeding microstrip line of the antenna as illustrated in figure 2.34.

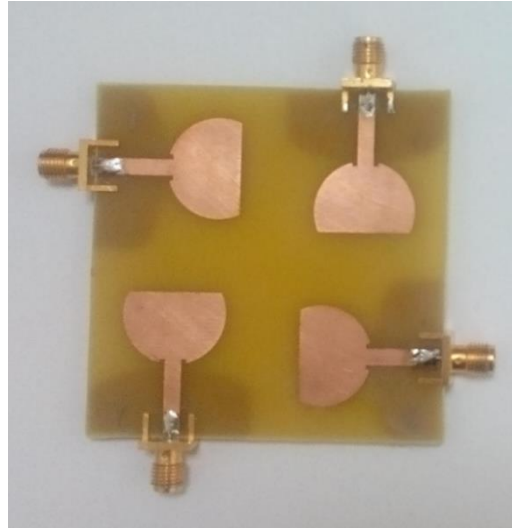


Figure 2. 35 prototype after soldering the connectors

The measurements were performed in CDTA (Centre de Développement des Technologies Avancées), Baba Hassen – Algiers where we have accomplished an internship working on this project

Keysight network analyzer was used to measure magnitude S-parameter of the antenna. Automatic calibration of the measuring cables was performed to eliminate the effect of cables on measurements, either in phase delay or losses.

The measuring cables do not have good flexibility. Thus when measuring a reflection coefficient, the concerned port is connected to the network analyzer and the other ports are loaded with 50Ω . Furthermore, when measuring transmission coefficients, the concerned two ports are connected to the network analyzer and the two others are 50Ω loaded as shown in the figure 2.36.

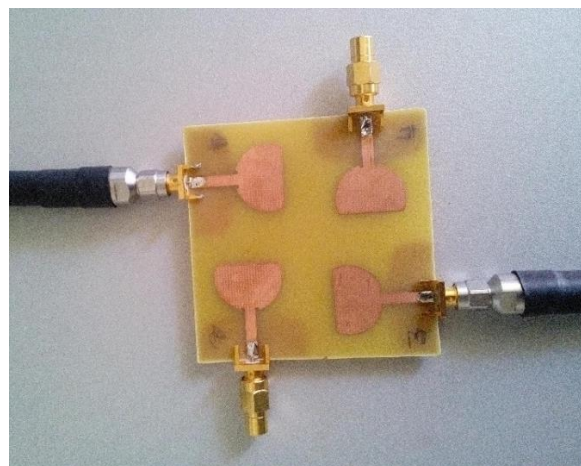


Figure 2. 36 Setup for two ports reflection coefficients measurement

The obtained results were recorded for a frequency range extending from 2 GHz to 12 GHz using 400 samples. The measured and simulated results of each pair of connected ports are illustrated in figures 2.37 and 2.38.

As the whole antenna system is symmetric, only the S-parameter of antenna “1” is measured. During measurement, when one port is considered the others are terminated with a standard 50-Ω matching load.

From figure 2.37, all measured $|S_{ij}|_{i \neq j}$ (transmission) parameters are less than -15 dB, therefore, all ports are isolated.

The following table represents the operating frequencies measured at each port as extracted from measured S-parameter curves.

Table 2.1: operating band of the manufactured antenna

| Port | Operating bands |
|--------|---------------------------|
| Port 1 | 3.5→8.28 GHz |
| Port 2 | 3.26→9.27 GHz |
| Port 3 | 4.16→5.02 & 5.6→8.35 GHz |
| Port 4 | 2.53→3.35 & 4.32→8.75 GHz |

From the table 2.1 and figure 2.38, it is observed that the bandwidths of all ports are less than the desired UWB band especially at high frequencies. This can be explained by imperfections in the fabrication process: shifting of the ground plane, introducing of SMA connectors and the welding of the prototype as well as the variation of relative permittivity substrate FR4 at high frequencies. However, the results are still acceptable since WiMAX frequencies (3.5 and 5.8 GHz) is covered by the fabricated antenna which make it a good candidate in smart grid applications.

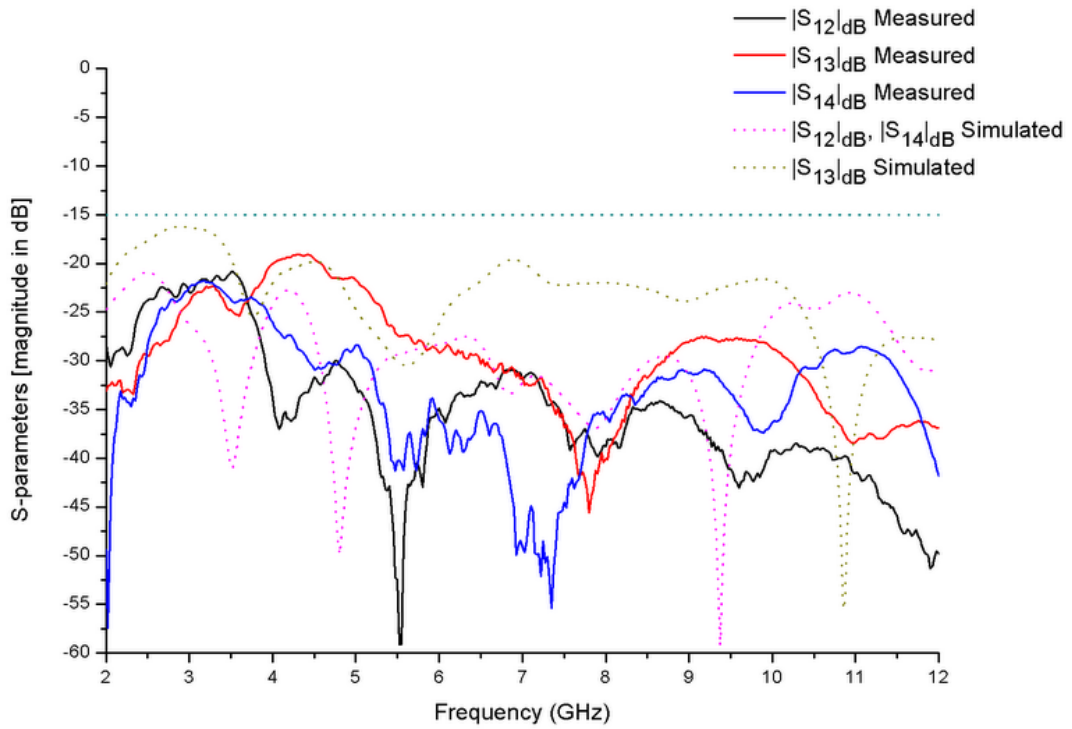


Figure 2. 37 Measured and simulated $|S_{ij}|_{i \neq j}$ coefficients

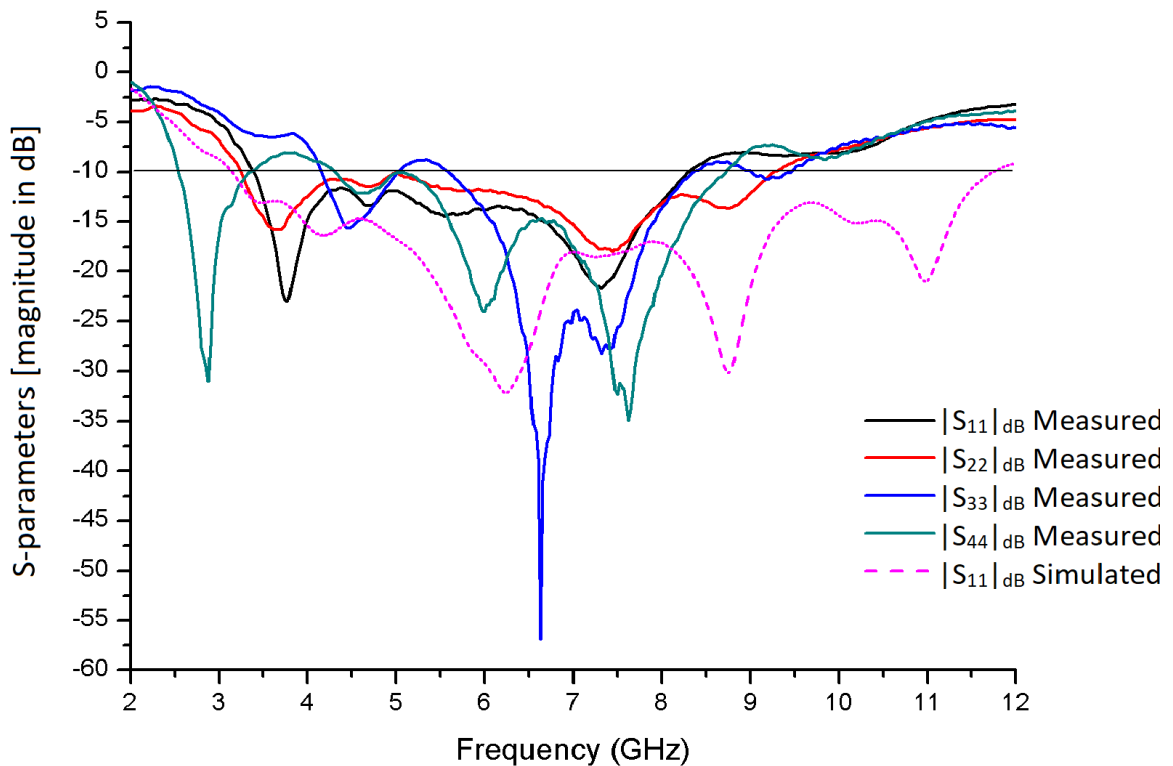


Figure 2. 38 Measured and simulated reflection coefficients

2. 6 Conclusion

Throughout this chapter, an UWB single antenna element has been developed and its radio electric characteristics investigated. After that, based on this basic element, different antenna MIMO configurations using 2 and 4 elements have been considered and their parameters involving isolation, correlation and diversity gains studied.

A 4-element final MIMO antenna configuration has been selected and a prototype fabricated and its S-parameters measured. This structure has been found that it fits the intended application in smart grids network.

Dual Band MIMO Antenna

3.1 Introduction

The objective of this chapter is the design of a Dual Band antenna that covers WiMAX frequency of 3.5 GHz as well as Wi-Fi 5GHz band which are used in smart grids systems. This starts by considering a single element whose prosperities are improved with a parametric study. After that a four-element MIMO configuration is investigated.

3.2 Design and simulations of the reference element

The basic square coplanar monopole antenna printed on an FR4 glass epoxy substrate is presented in figure 3.1. It consists of two radiating patches to achieve resonance at the desired frequencies.

To obtain adequate antenna dimensions, the effects of the gap h , the ground plane length G_l and the substrate length S_l which affect strongly the antenna behavior as will be shown by the corresponding reflection coefficients illustrated here after are investigated. The other antenna dimensions used in this parametric analysis are shown in the figure 3. 1.

Accordingly, the effects of the parameters h , G_l and S_l are shown by figures 3.2-4 respectively which confirm the strong effects of these parameters on the resonant frequencies as well as the antenna bandwidths characteristics.

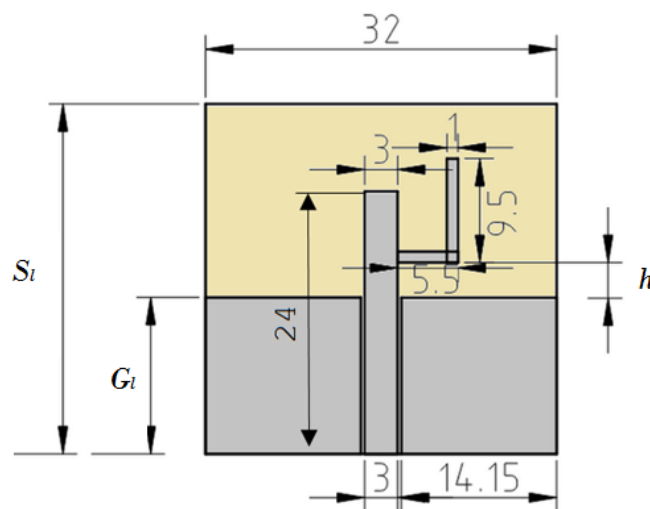


Figure 3. 1 Basic Dual Band antenna element geometry

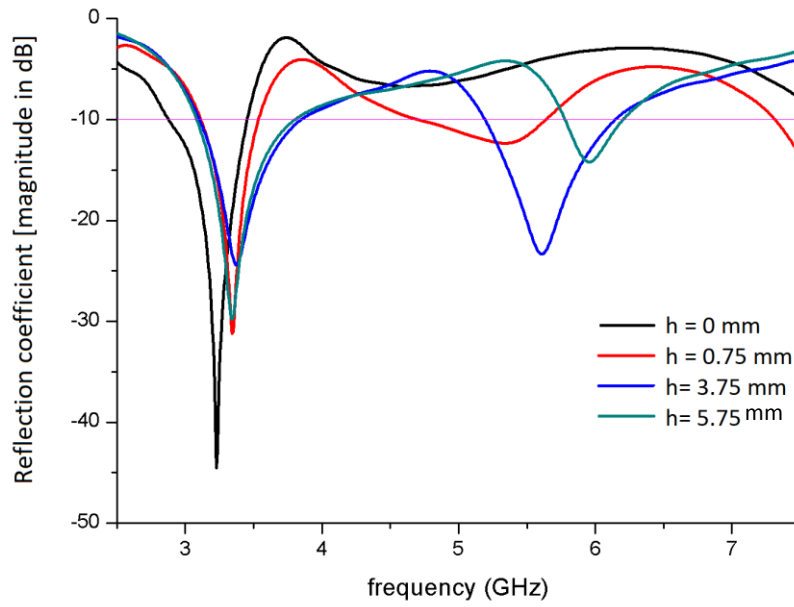


Figure 3. 2 Simulated reflection coefficient of the microstrip antenna for different feed gaps h With $G_L=12$ mm and $S_L=28$ mm.

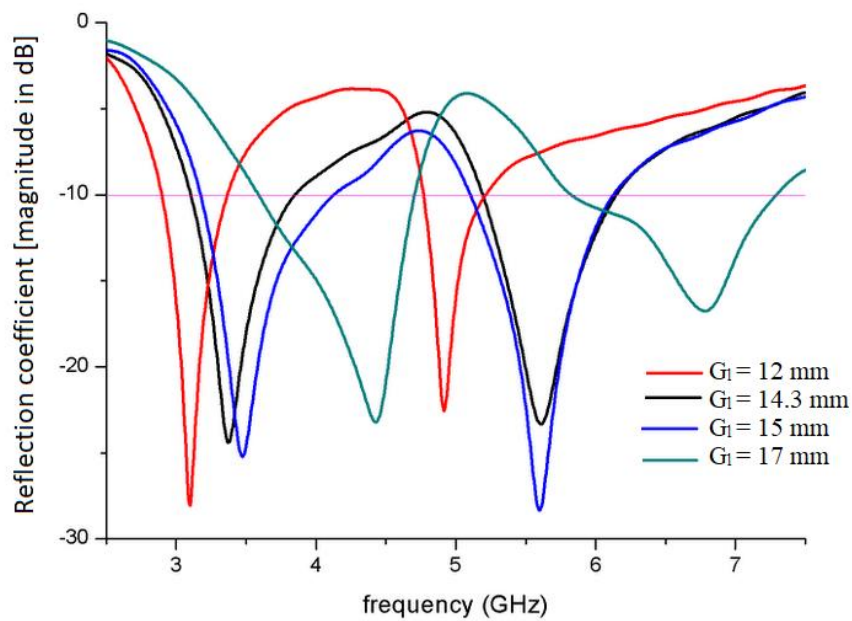


Figure 3. 3 Simulated reflection coefficient of the microstrip antenna for different G_L with $h=3.75$ mm $S_L=28$ mm

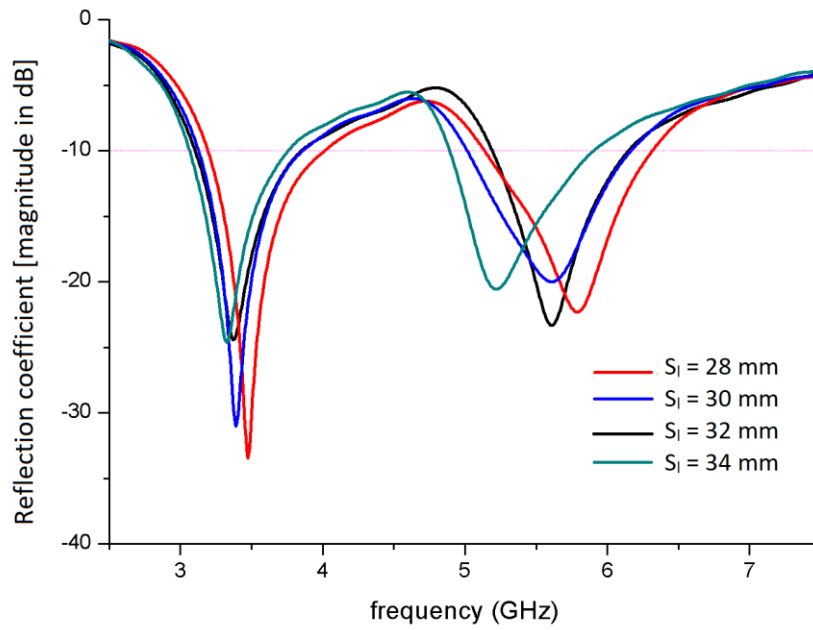


Figure 3. 4 Simulated reflection coefficient of the microstrip antenna for different S_l with $h=3.75$ mm and $G_l=14.3$ mm

In light of the parametric study, the reference antenna geometrical dimensions operating around the specified frequencies with best bands characteristics are shown in figure 3.5.

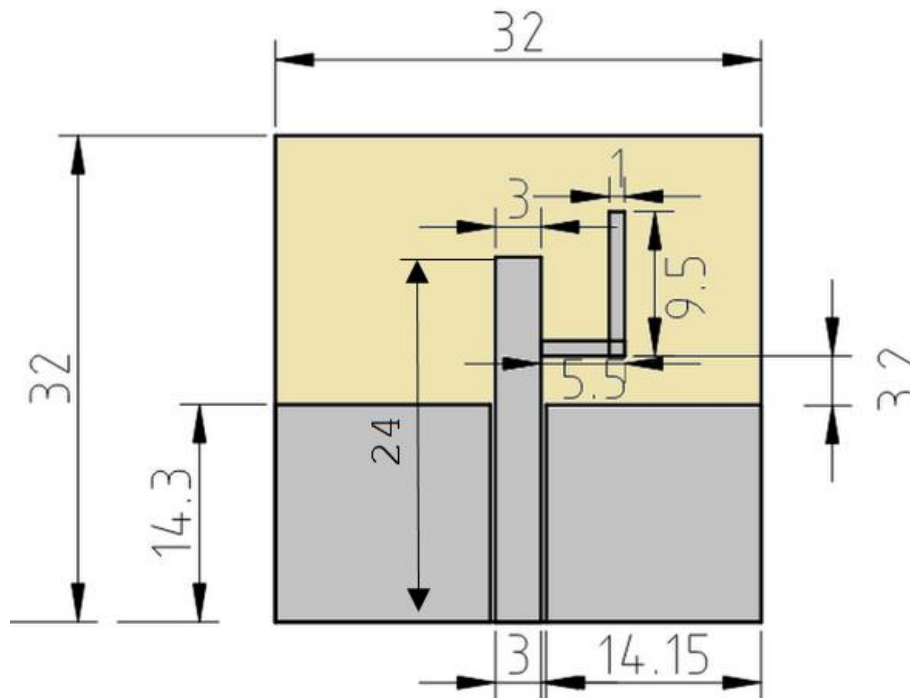


Figure 3. 5 Final Dual Band antenna element geometry

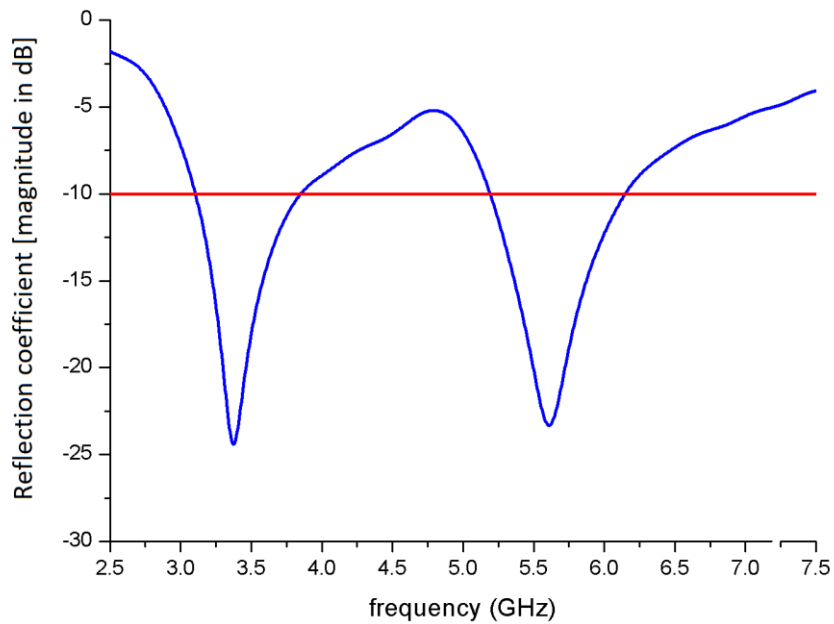


Figure 3. 6 Reflection coefficient of the basic Dual Band antenna

The simulated reflection coefficient shows two frequency bands, [3.1–3.8 GHz] and [5.09–6.1 GHz], which meet the desired bandwidths.

Figure 3.7 represents the peak gain versus frequency of the dual band element. It is seen in this figure that the peak gain has an acceptable and a relatively stable level in the operating bands which makes the antenna suitable for the intended application.

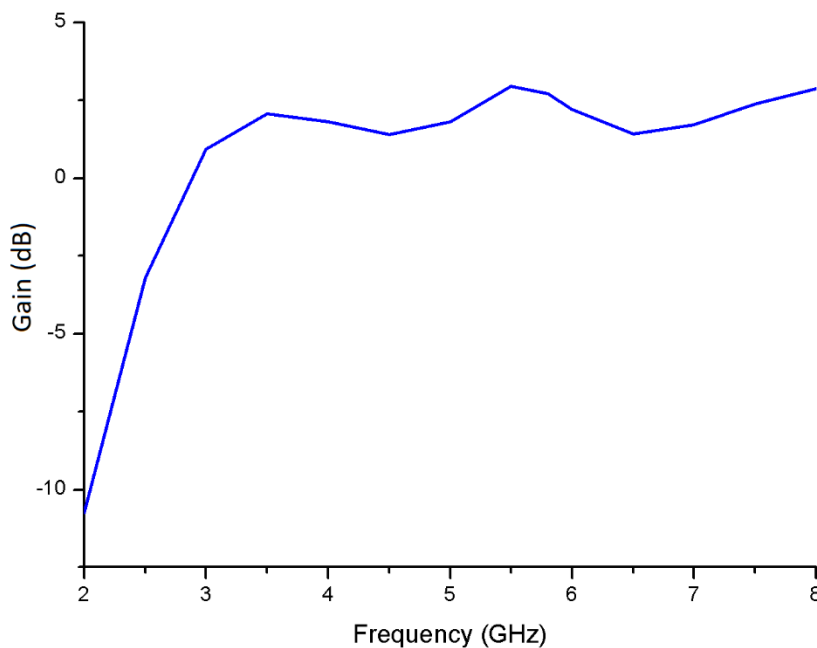
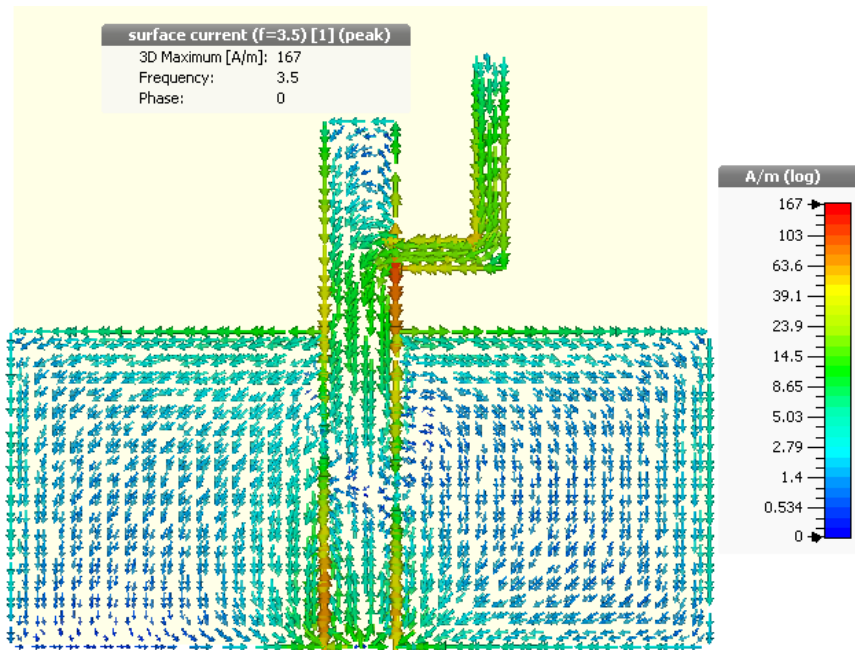
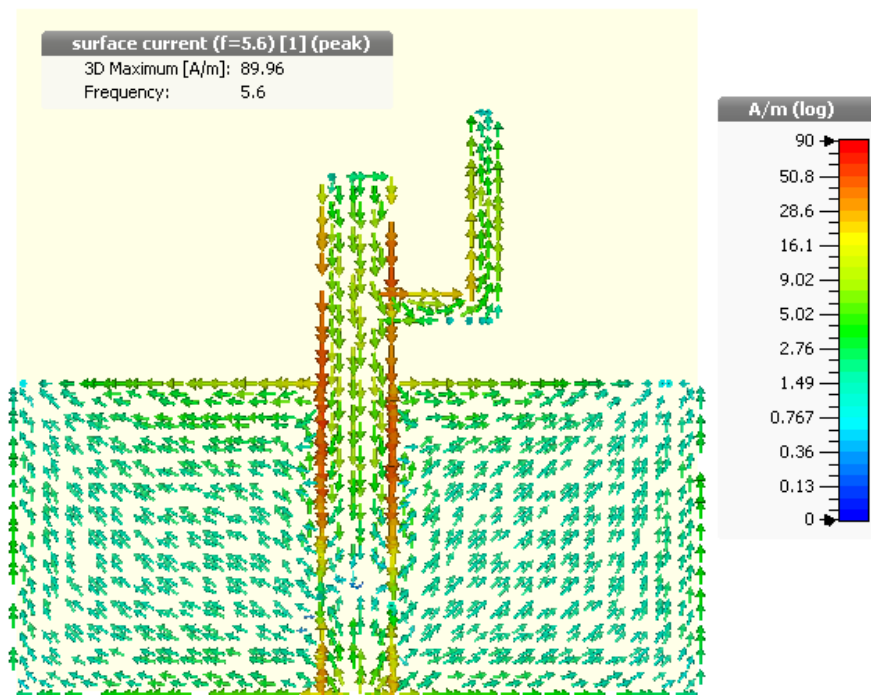


Figure 3. 7 Simulated gain vs. frequency of the reference Dual Band antenna

Figure 3.8 shows the average current density distribution near the resonances, at 3.5 GHz and the second resonance at 5.6 GHz.



(a) $f = 3.5$ GHz



(b) $f = 5.6$ GHz

Figure 3. 8 Surface current distribution of the reference Dual Band antenna

It is seen from these figures that the current density is mainly concentrated along the microstrip feeding line and the right side radiator for the low resonance (3.5 GHz) and along the shortest radiator for the higher resonance (5.6 GHz).

The 3-D and the 2-D radiation patterns in the planes $\Phi=0^\circ$ and $\Phi=90^\circ$ at the frequencies 3.5 and 5.6 GHz are illustrated in Figures 3.9-10.

These figures indicate that the pattern is quasi omnidirectional for the frequency 3.5 GHz and consists mainly of two lobes for the frequency 5.6 GHz.

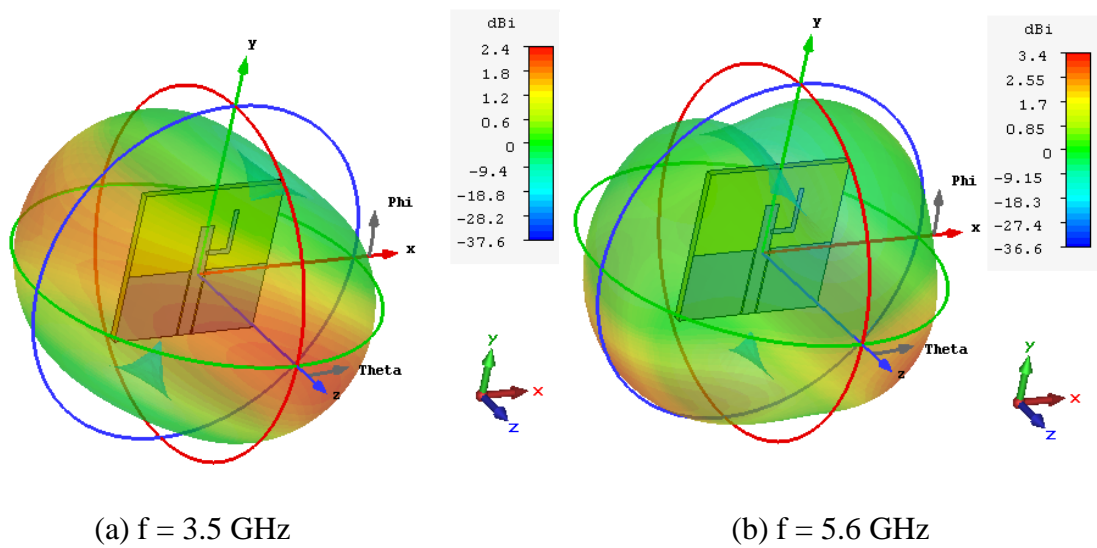


Figure 3. 9 3-D Radiation pattern of the reference Dual Band antenna

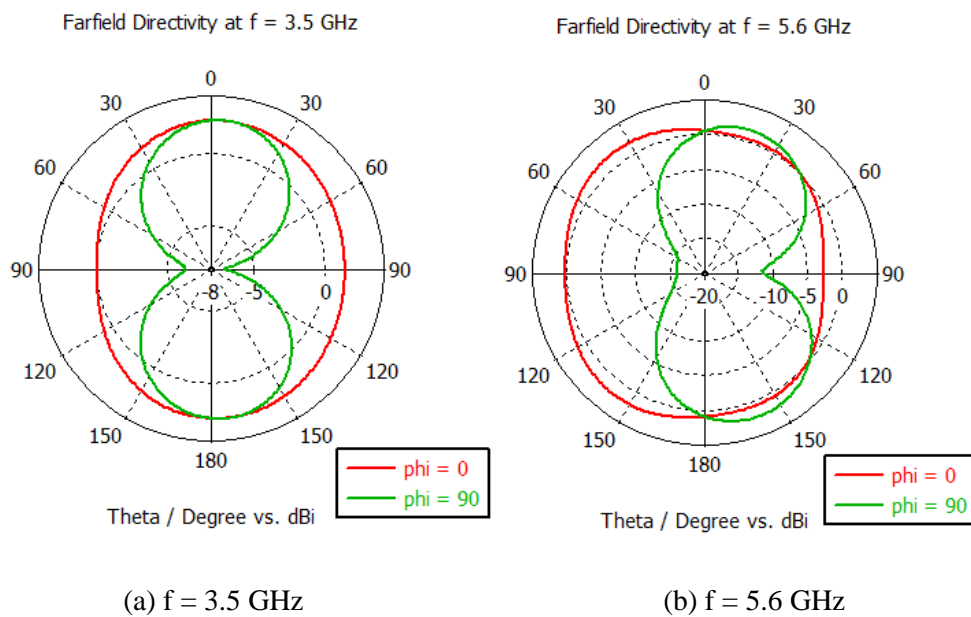


Figure 3. 10 2-D Radiation pattern of the reference Dual Band antenna at frequencies 3.5 and 5.6 GHz

3.3 Design and simulation of four-element MIMO antenna

The MIMO configuration considered in this section consists of four antenna basic elements arranged orthogonally as shown in figure 3.11. Since a single antenna is square, the total size of the 2x2 MIMO configurations is 6.4×6.4 mm².

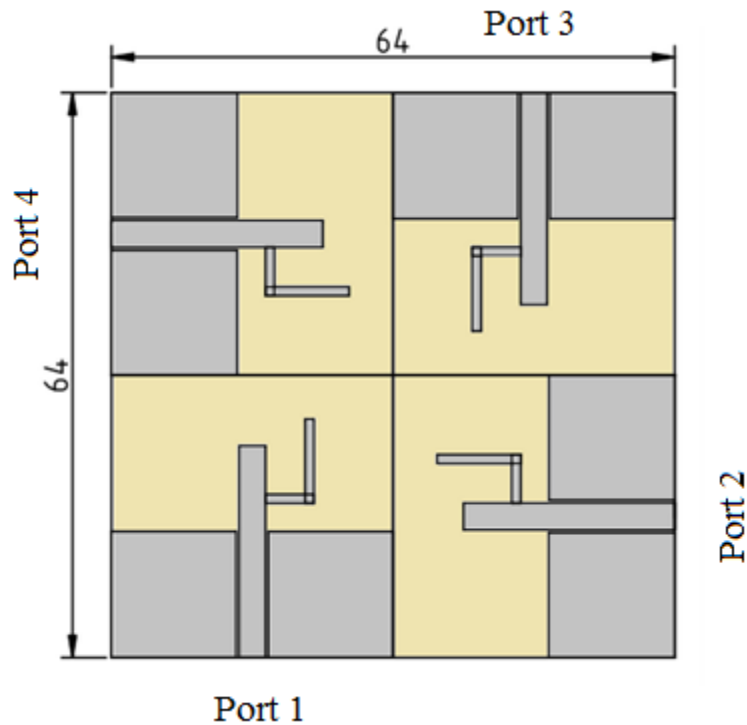


Figure 3. 11 Configuration of the 4-element Dual Band MIMO antenna

Due to the configuration symmetry, the S-parameters verify the following relationships:

$$x \quad S_{11} = S_{22} = S_{33} = S_{44}.$$

$$x \quad S_{12} = S_{21} = S_{23} = S_{32} = S_{34} = S_{43} = S_{41} = S_{14}$$

$$x \quad S_{13} = S_{31} = S_{24} = S_{42}.$$

Consequently, the S-parameters simulation is limited to the parameters indicated in the left side of the above equations. Accordingly, the obtained results are illustrated in figure 3.12.

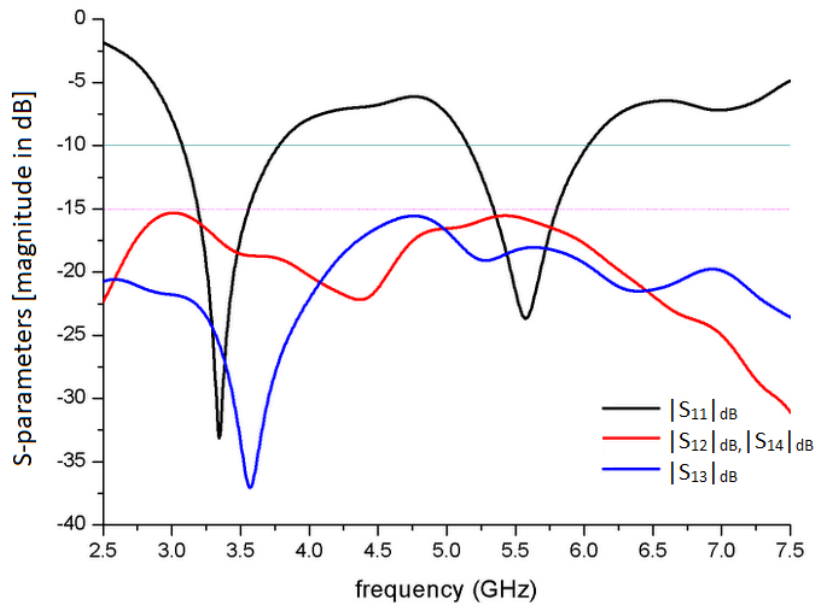


Figure 3. 12 S-parameters of the 4-element Dual Band MIMO Antenna

The reflection coefficient graph $|S_{11}|_{dB}$ indicates that the operating frequency bands are 3.16-3.75 GHz and 5.19-6.05 GHz which fit the Wi-Fi/WiMAX for Smart Grid applications. Furthermore, all elements are well isolated since $|S_{ij}|_{i \neq j}$ dB levels are less than -15 dB.

Figure 3.13 represents the 4-element Dual Band antenna gain versus frequency. It is shown that gain is enhanced compared to the gain of the reference antenna.

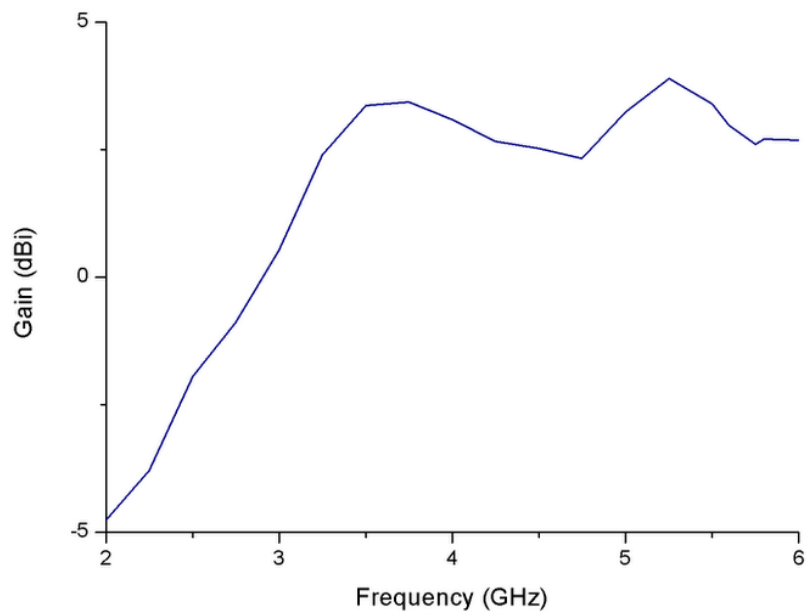


Figure 3. 13 Simulated gain vs. frequency of the 4-element Dual Band MIMO antenna

Figures 3.14-17 show the correlation coefficients and the diversity gains between adjacent and oblique ports.

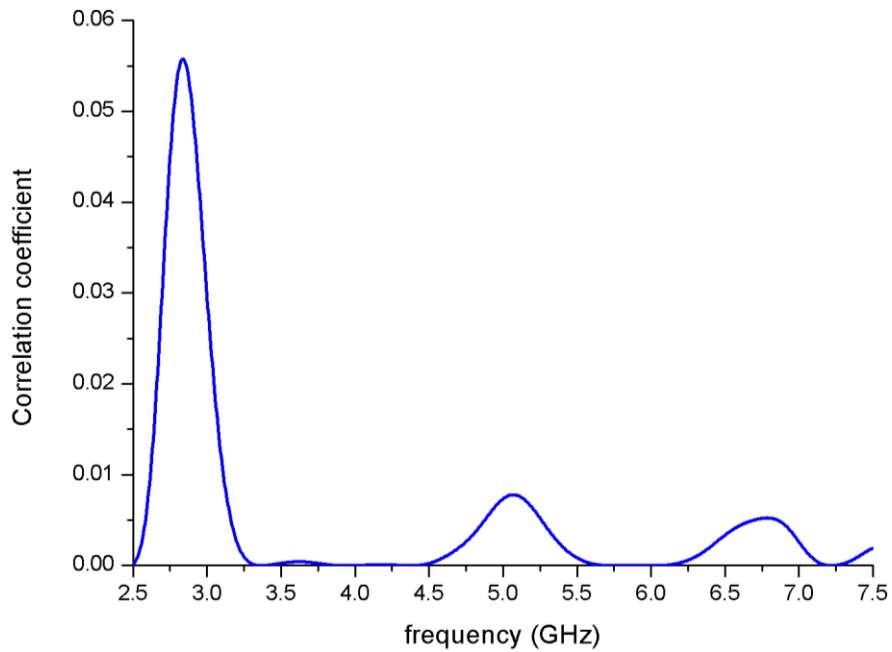


Figure 3. 14 Correlation coefficient between adjacent ports

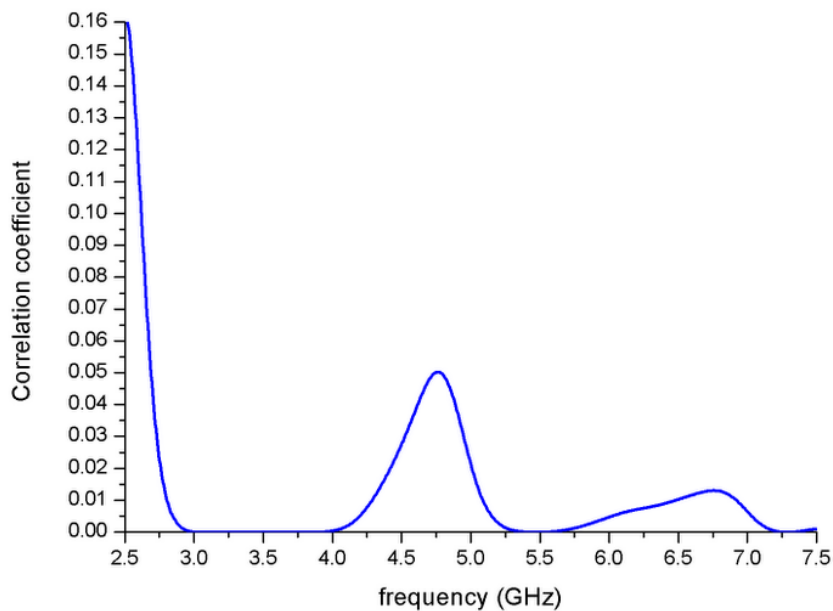


Figure 3. 15 Correlation coefficient between oblique ports

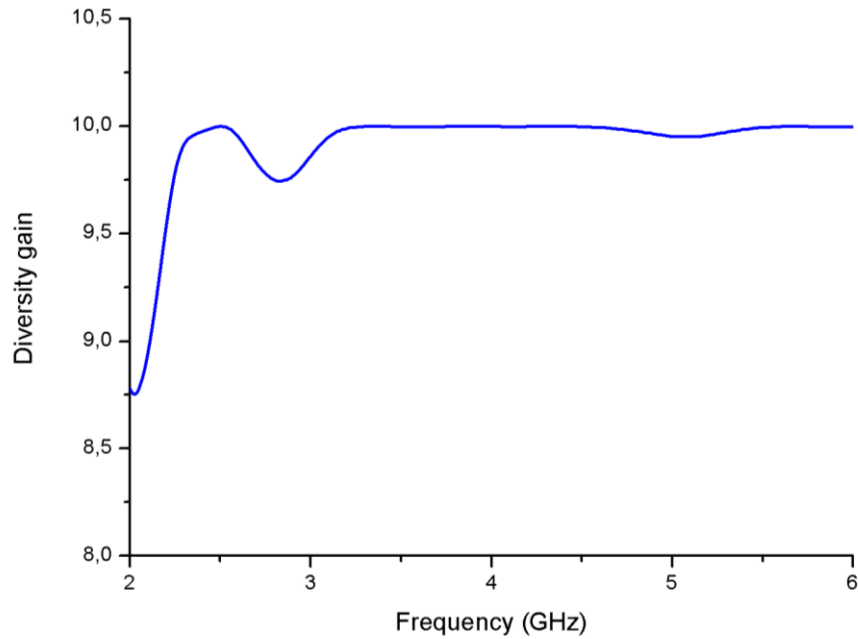


Figure 3. 16 Diversity gain between adjacent ports

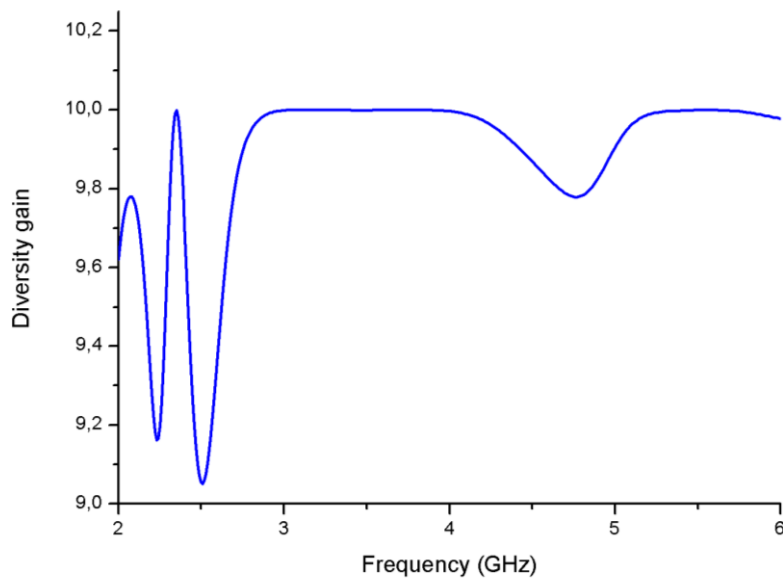
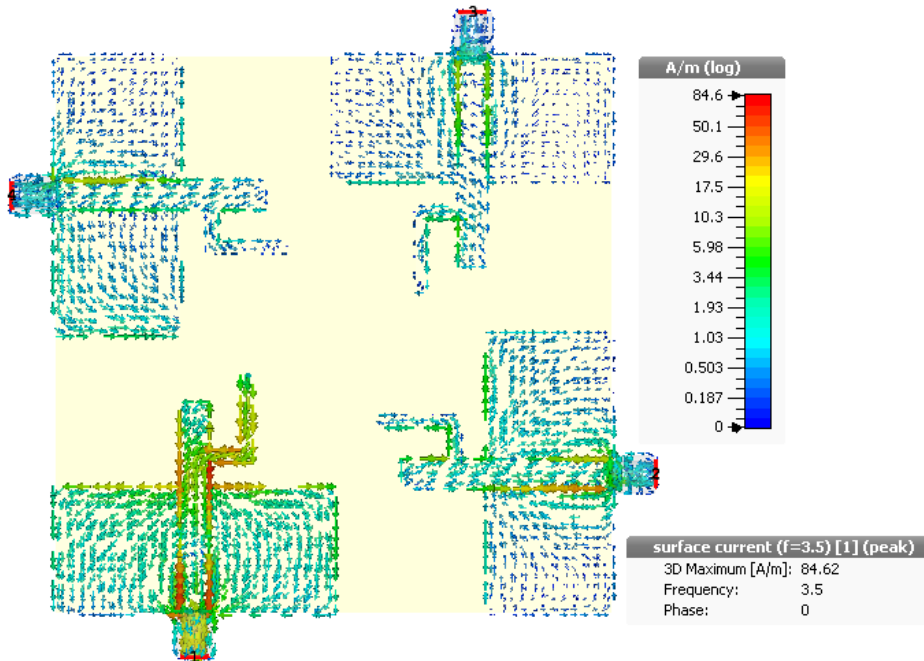


Figure 3. 17 Diversity gain between oblique ports

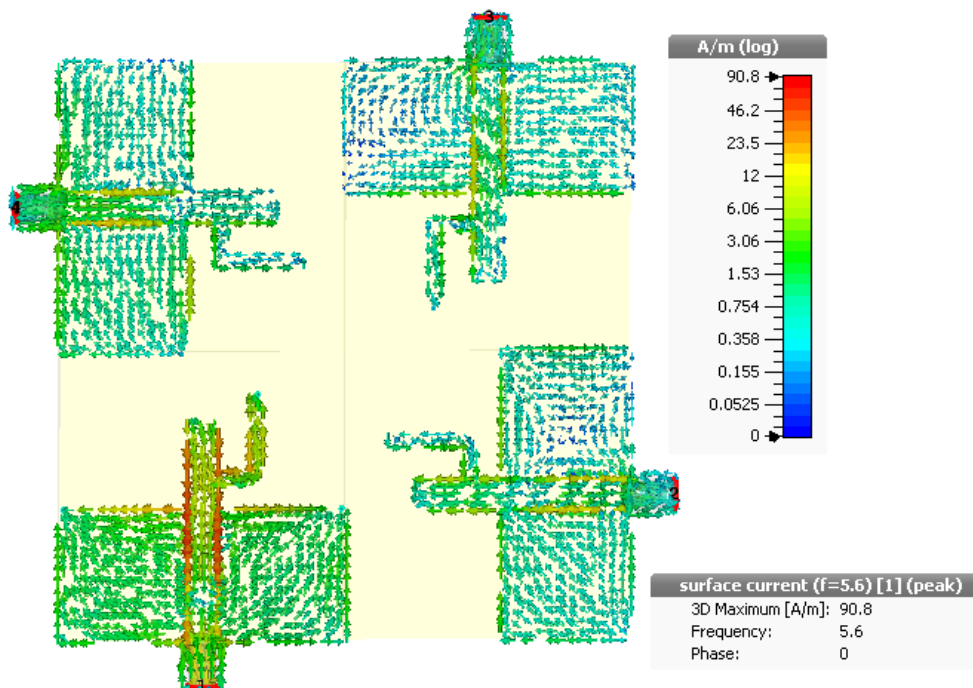
From the above figures, it is observed that the envelope correlation coefficient is very low at the desired frequency bands (less than 0.1) whereas the diversity gain is greater than 9.9 which denote a good isolation between adjacent and oblique elements of the MIMO system.

The surface current distributions on the four elements when exciting “port 1” at frequencies 3.5 and 5.6 GHz are illustrated in figure 3.18. This figure indicates clearly the current path involved in each of these frequencies. As expected, this path includes the main radiator length

at the frequency 5.6 GHz (shorter path) and, a part of this radiator along with the right side radiator (longer path) at 3.5 GHz.



(a) $f = 3.5$ GHz



(b) $f = 5.6$ GHz

Figure 3. 18 Surface distribution current of 4-element Dual Band MIMO antenna

The following figures represent 3-D and polar radiation pattern for the four element MIMO antenna at “port 1”.

At the frequency 3.5 GHz, the pattern exhibits in the plane $\Phi=0^\circ$ a main lateral lobe in the direction $\Theta=0^\circ$ and two lobes in the plane $\Phi=90^\circ$. At the frequency 5.6 GHz, the pattern consists of many lobes in the plane $\Phi=0^\circ$ and two lobes, one in each side of the x-y plane.

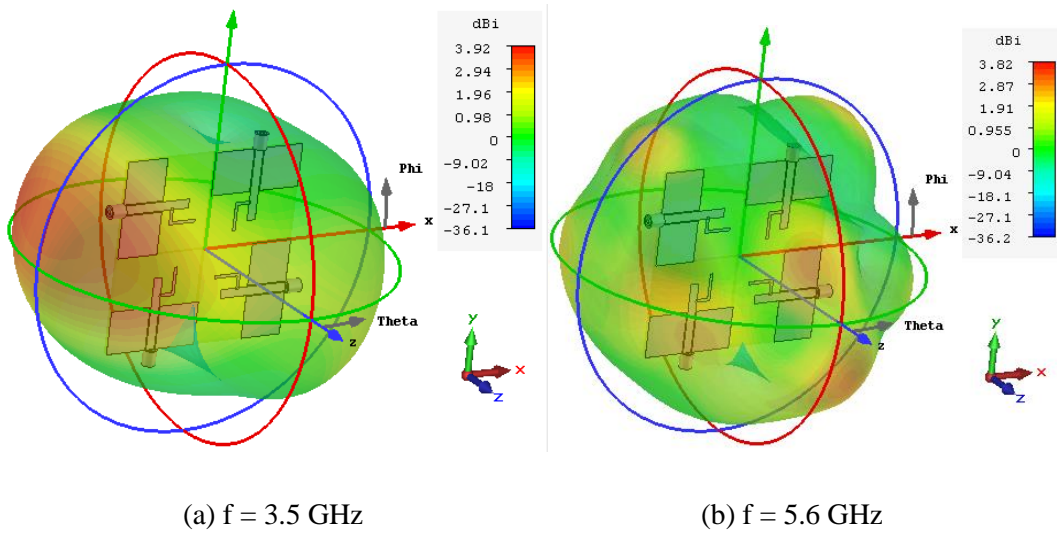


Figure 3. 19 3-D radiation pattern of the Dual Band MIMO antenna

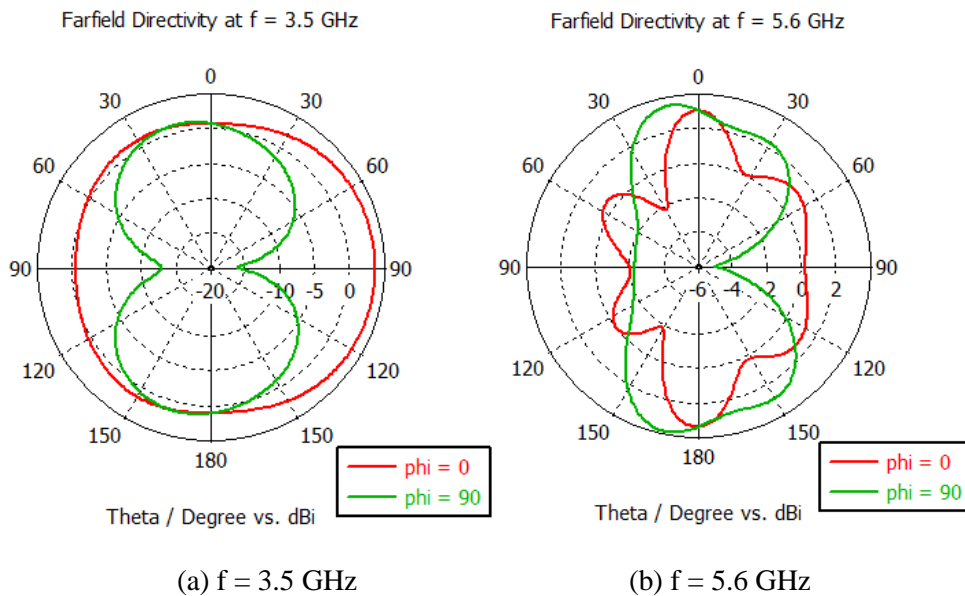


Figure 3. 20 2-D radiation pattern at different frequencies when exciting “port 1”

3.4 MIMO antenna system prototypes measurements

The fabrication of the 2×2 MIMO antenna prototype was performed in SNC ALMITech laboratory in Kouba (Algiers).

A photograph of the manufactured structure is shown in figure 3.21.

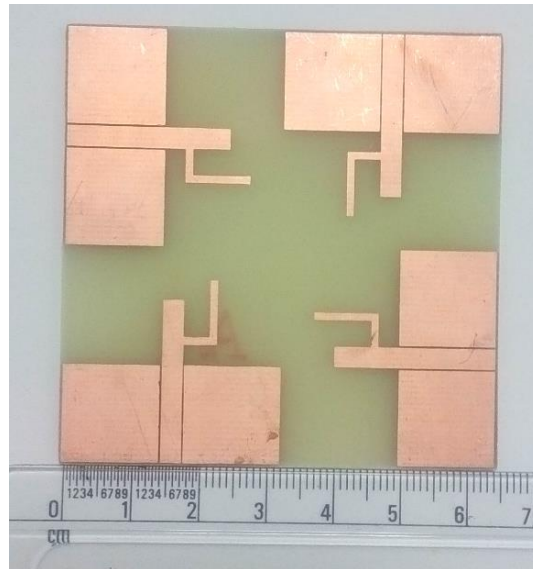


Figure 3. 21 Manufactured Dual Band 2×2 MIMO antenna

Four SMA connectors (50-Ohm characteristic impedance) were welded to each feeding microstrip line of the antenna as illustrated in figure 3.22.

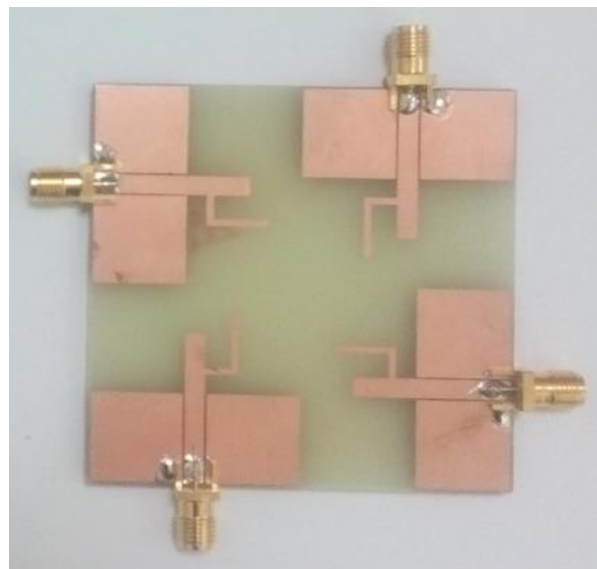


Figure 3. 22 Antenna prototype after soldering the connectors.

The measurements were performed in CDTA (Centre de Développement des Technologies Avancées), Baba Hassen – Algiers where we have accomplished an internship working on this project.

The measured S-parameters, illustrated in figure 3.24, indicate that the ports are isolated since all $|S_{ij}|_{i \neq j}$ parameters are less -15 dB.

Moreover, the reflection coefficient at frequencies 3.5 GHz and 5.6 GHz are found to be less than -13dB and -25 dB respectively. Furthermore, the measurement results achieve satisfactory bandwidths characteristics cover the dual frequency bands of 3.1 to 3.8 GHz for WiMAX and 5.0 to 5.8 GHz for Wi-Fi systems.

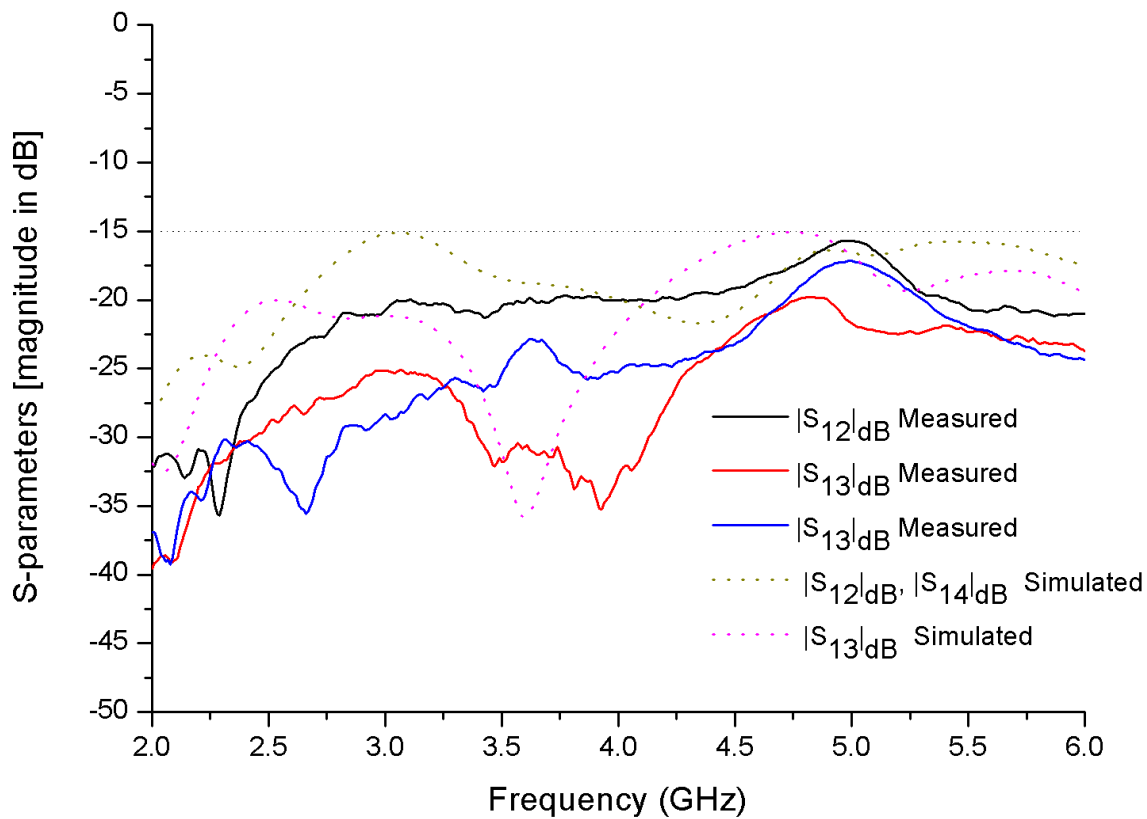


Figure 3. 23 Measured and simulated $|S_{ij}|_{i \neq j}$ parameters

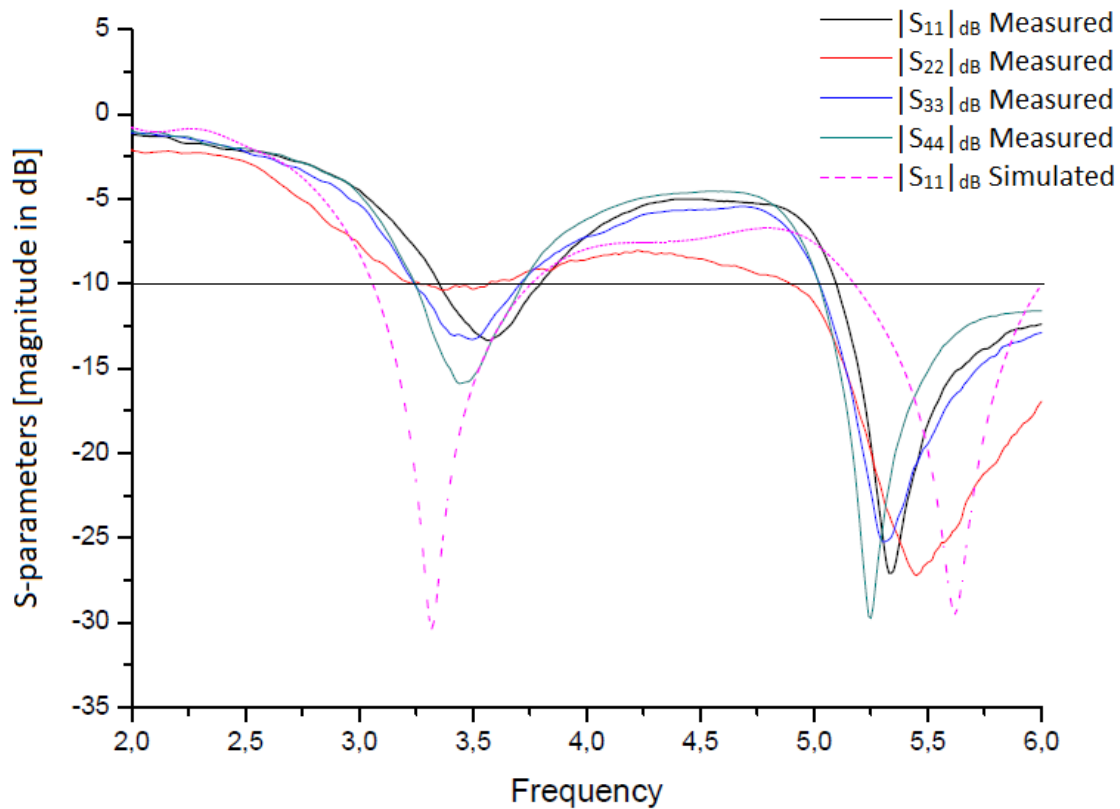


Figure 3. 24 Measured and simulated reflection coefficients

Finally, Figure 3.25 shows a comparison between simulated and measured results for the S_{ii} parameters. It is noticed that the antenna operates at 3.5 and 5.6 GHz at all ports with a slight shift of the resonant frequencies. A difference is also recorded on the minimum reflection coefficient levels though the antenna bandwidths are still satisfactory with respect to the desired band characteristics. These differences are due to several parameters such as errors in the fabrication process and, imperfections in soldering which affect the contact between the SMA connectors and the antenna feed line.

3.4 Conclusion

In this chapter, a dual band single antenna element has been developed and its radio electric characteristics investigated. After that, based on this basic element, a 2x2 MIMO configuration has been considered and its radio electric prosperities including isolation, correlation and diversity gains studied.

A prototype of the developed 4-element final dual band MIMO antenna has been fabricated and its S-parameters measured. This structure has been verified to fit the intended application as it operates in the 3.5 GHz WiMAX and the 5.6 GHz Wi-Fi bands used in smart grid systems.

General Conclusion

This work presents two MIMO antenna configurations that can be incorporated in wireless communication systems operating in Wi-Fi/WiMAX frequency bands used in Smart Grid applications.

These MIMO configurations are respectively based on an UWB and a Dual Band basic elements. These structures, mounted on an FR-4 substrate layer, are fed by a microstrip line for the UWB and by a coplanar waveguide for the Dual Band antenna.

For each of the proposed configurations, the analysis starts by considering the basic antenna element whose band characteristics are enhanced and the radio electric prosperities, including the current distribution and the radiation patterns, investigated.

After that, different MIMO antenna configurations, using two and four elements for the UWB structure and four elements for the Dual Band antenna, have been investigated. Besides, the classical antenna parameters listed above, the analysis concerned also isolation, correlation coefficient and diversity gain which are important parameters in MIMO antenna systems.

The analysis, carried out using the CST Microwave Studio simulator, ended up with two final 2x2 MIMO antennas based respectively on the UWB and the Dual Band basic elements and suitable for the intended application.

Within smart grid systems, the UWB MIMO antenna can be used in the WiMAX (3.5 GHz and 5.8 GHz) bands and, the Dual Band configuration in the WiMAX (3.5 GHz) and the Wi-Fi (5.6 GHz) bands.

Prototypes of the two four-element MIMO antennas have been fabricated and their S-parameters measured where an agreement is observed between simulated and measured results.

References

- [1] <https://www.mobilemark.com/how-smart-grid-technology-antennas-drive-smart-grid-coverage/>
- [2] P. Rengaraju, C. H. Lung, A. Srinivasan, "Communication Requirements and Analysis of Distribution Networks using WiMAX Technology for Smart Grids", *2012 8th International Wireless Communications and Mobile Computing Conference (IWCMC)*, 2012.
- [3] L. Li, H. Xiaoguang, C. Ke, and H. Ketai, "The applications of Wi-Fi based wireless sensor network in Internet of things and smart grid," in Proc. 6th IEEE Conf. Ind. Electron. Appl. (ICIEA), Beijing, China, 2011.
- [4] PCTEL, "www.fliphtml5.com," 11 October 2015. [Online]. Available: <http://fliphtml5.com/miqg/prmk/basic>.
- [5] C. L. J. W. Nick Jenkins, "An Overview of the Smart Grid in Great Britain," *Engineering*, vol. 1, no. 4, pp. 401-512, 2015.
- [6] J. Ekanayake, K. Liyanage, J. Wu, A. Yokoyama, N. Jenkins, "Smart Grid: Technology and Applications", John Wiley & Sons, Ltd., Chichester (2012)
- [7] N. Jenkins, J.B. Ekanayake, G. Strbac, Distributed Generation, the Institution of Engineering and Technology, London (2010)
- [8] T. Vijayapriya and D. Kothari, "Smart Grid: An Overview," *Smart Grid and Renewable Energy*, Vol. 2 No. 4, 2011, pp. 305-311.
- [9] V. C. Gungor, L. Bin, and G. P. Hancke, "Opportunities and challenges of wireless sensor networks in smart grid," *IEEE Trans. Ind. Electron.*, vol. 57, no. 10, pp. 3557–3564, 2010.
- [10] V. C. Gungor, D. Sahin, T. Kocak, et al., "Smart grid technologies: communication technologies and standards", *IEEE Trans. Ind. Inform.* 7(4), 529–539 (2011).
- [11] Ruhul .A, Mahmudul .H, Rajib B.R, "Roadmap To Smart Grid Technology: A Review of Smart Information and Communication System", *International Journal of Control and Automation*, Vol. 7, No.8, Pp. 407-418, 2014
- [12] IEEE Standard for Wireless MAN-Advanced Air Interface for Broadband Wireless Access Systems, 7 September 2012
- [13] <https://www.electronics-notes.com/articles/connectivity/wimax/frequencies-spectrum-bands.php>

- [14] Trevor S. Bird, "Fundamentals of Aperture Antennas and Arrays: From Theory to Design, Fabrication and Testing", Wiley; 1st edition (2016)
- [15] Constantine A. Balanis, "Antenna theory, analysis and design", Wiley, 3rd edition (2005)
- [16] P.Kokila, T.Saranya, S.Vanitha, "Analysis and Design of Rectangular Microstrip Patch Antenna Using HFSS", Journal of Network Communications and Emerging Technologies (JNCET), Volume 6, Issue 4, April (2016)
- [17] <http://www.patchantenna.blogspot.com>
- [18] By D. Orban and G.J.K. Moernaut, "The Basics of Patch Antennas", the RF Globalnet newsletter, September (2009).
- [19] SK Behera, "Novel Tuned Rectangular Patch Antenna as a load for phase Power combining," PhD Thesis, Jadupur University, Kolkata (2007).
- [20] N.Lalam and MaitriSomaniBangard, "Wireless Reception for Microcontroller based Sensor Networks," International Journal of Advanced Computation Engineering and Networking, Vol.1, no.10 (2013).
- [21] ABED Djamel, "Conception Réalisation et Caractérisation d'Antennes Imprimées pour les Communications Ultra Large Bande", thèse de Magistère (2009), Ecole Militaire Polytechnique.
- [22] M. PRASANNA.K, "DESIGN AND ANALYSIS OF TWO PORT MIMO ANTENNAS WITH WIDEBAND ISOLATION", Master thesis, Department of Electronics and Communication Engineering., National Institute of Technology Rourkela-769008, 2013.
- [23] S.Weigand, G.H. Huff, K.H. Pan, and J.T. Bernhard, "Analysis and Design of Broad-band Single Layer Rectangular U- Slot Microstrip Patch Antennas", IEEE Trans. Antennas and Propag.,vol. 51, No.3, pp. 457-468, March, 2003.
- [24] Ali, M.; Okoniewski, M.; Stuchly, M. A Stuchly, M. M. "Dual-Frequency Strip-Sleeve Monopole for Laptop Computers, IEEE Transactions on Antennas and Propagation", Vol.47, No. 2, February 1999.
- [25] Prasanna, K M, Behera, S K, "A Hexagonal MIMO Antenna System With Defected Ground Structure to Enhance Bandwidth and Isolation", IEEE International Conference on Communication & Signal Processing, ICCSP-2013, April 3-5, 2013.
- [26] Istvan Szini, Alexandru Tatomirescu, and Gert Frølund Pedersen, "On Small Terminal MIMO Antennas, Harmonizing Characteristic Modes with Ground Plane Geometry", IEEE Transactions on Antennas and Propagation · April 2015
- [27] Chirag R. Shah, " Performance and Comparative Analysis of SISO, SIMO, MISO, MIMO", International Journal of Wireless Communication and Simulation, Volume 9, Number 1 (2017)

- [28] M. PRASANNA.K, DESIGN AND ANALYSIS OF TWO PORT MIMO ANTENNAS WITH WIDEBAND ISOLATION, Department of Electronics and Communication Engineering: A Thesis submitted in partial fulfillment of the Requirements for the degree of MASTER OF TECHNOLOGY IN COMMUNICATION AND SIGNAL PROCESSING, 2013.
- [29] S. Plevel, S. Tomazic, T. Javornik, and G. Kandus, "MIMO: Wireless communications," Encyclopedia of Wireless and Mobile Communications, 2008.
- [30] I. Stevanovic, A. Skrivervik, and J. R. Mosig, "Smart antenna systems for mobile communications," Tech. Rep., 2003.
- [31] E. Mohamed and A. Abdulsattar, "Evaluation of mimo system capacity over rayleigh fading channel." International Journal of Computer Science and Engineering Survey (IJCSSES).2015
- [32] N. Janssen, K. A. Remley, C. L. Holloway, and W. F. Young, "Correlation coefficient and loading effects for mimo antennas in a reverberation chamber," in Electromagnetic Compatibility (EMC EUROPE), 2013 International on. IEEE, 2013.
- [33] A. I. Najam, S. Tedjini, and Y. Duroc, "Multiple-input multiple-output antennas for ultra-wideband communications", INTECH Open Access Publisher, 2012.